





RESEARCH ARTICLE

Paclitaxel in vitro reversibly sensitizes the excitability of IB4(–) and IB4(+) sensory neurons from male and female rats

Eva Villalba-Riquelme¹  | Roberto de la Torre-Martínez²  |
Asia Fernández-Carvajal¹  | Antonio Ferrer-Montiel¹ 

¹Instituto de Investigación, Desarrollo e Innovación en Biotecnología Sanitaria de Elche (IDiBE), Universitat Miguel Hernández, Elche, Spain

²Department of Neuroscience, Karolinska Institutet, Stockholm, Sweden

Correspondence

Antonio Ferrer-Montiel, IDiBE-UMH, Av. De la Universidad s/n. 03202 Elche, Spain.
Email: aferrer@umh.es

Funding information

Generalitat Valenciana (GVA), Grant/Award Numbers: IDIFEDER 2018/20, PROMETEO/2021/031; Ministerio de Ciencia, Innovación y Universidades (MCIU), Grant/Award Numbers: RTC-2017-6507-1, RTI2018-097189-B-C21; Universidad Miguel Hernández (UMH), Grant/Award Number: PAR2019

Background and Purpose: Paclitaxel produces a chemotherapy-induced peripheral neuropathy that persists in 50–60% of cancer patients upon treatment. Evidence from animal models suggests an axonopathy of peripheral A- and C-type fibres that affects their excitability. However, direct effects of paclitaxel on sensory neuron excitability and sexual dimorphism remain poorly understood.

Experimental Approach: We used a long-lasting (10 days in vitro) primary culture of rat dorsal root ganglion (DRG) neurons to investigate the time course effect of paclitaxel on the electrical activity of IB4(–) and IB4(+) sensory neurons of female and male adult Wistar rats.

Key Results: Paclitaxel strongly and reversibly stimulated spontaneous activity and augmented action potential tonic firing in IB4(–) and IB4(+) neurons in both sexes, peaking at 48 h post-treatment and virtually disappearing at 96 h. Paclitaxel decreased the current rheobase for action potential firing by reducing and accelerating the after-hyperpolarization phase. Molecularly, paclitaxel modulated Na⁺ and K⁺ ion currents. Particularly, the drug significantly augmented the function of Na_v1.8, TRPV1 and TRPM8 channels. Furthermore, paclitaxel increased Na_v1.8 and TRPV1 expression at 48 h post-treatment. Notably, we observed that female DRG neurons appear more sensitive to paclitaxel sensitization than their male counterparts.

Conclusions and Implications: Our data indicate that paclitaxel similarly potentiated IB4(–) and IB4(+) electrogenicity and uncover a potential sex dimorphism in paclitaxel-induced chemotherapy-induced peripheral neuropathy. Our in vitro, pre-clinical, chemotherapy-induced peripheral neuropathy paradigm provides a tool for studying the dynamics and underlying molecular mechanisms contributing to nociceptor sensitization in peripheral neuropathies and for testing desensitizing compounds.

Abbreviations: AHP, after-hyperpolarization phase; AITC, allyl isothiocyanate; AP, action potential; CIPN, chemotherapy induced peripheral neuropathy; DIV, days in vitro; DRG, dorsal root ganglion; G-V, conductance–voltage relationship; IB4, isolectin B4; iPSC, induced pluripotent stem cells; J-V, Current density–voltage relationship; K_A, fast-inactivating potassium current; K_{DR}, delayed-rectifier potassium current; MEA, microelectrode array; RMP, resting membrane potential; Rpl29, ribosomal protein L29; SA, spontaneous activity; t_{AHP}, time to recover from the AHP; t_{peak}, time to reach the maximum amplitude; t_r, repolarization time; TTX, tetrodotoxin; V_{th}, voltage threshold.

This is an open access article under the terms of the Creative Commons Attribution-NonCommercial-NoDerivs License, which permits use and distribution in any medium, provided the original work is properly cited, the use is non-commercial and no modifications or adaptations are made.

© 2022 The Authors. *British Journal of Pharmacology* published by John Wiley & Sons Ltd on behalf of British Pharmacological Society.

KEYWORDS

cancer, ion channel, neuropathy, nociceptor, pain, sexual dimorphism, thermoTRP

1 | INTRODUCTION

Paclitaxel is used as a first-line chemotherapeutic drug to treat several solid tumours (Abu Samaan et al., 2019; Markman, 1991;). This drug also induces a peripheral neuropathy (chemotherapy-induced peripheral neuropathy, CIPN), with a prevalence of up to 90% of patients during treatment that may persist for up to 48 months post-treatment (Colvin, 2019; Seretny et al., 2014). CIPN is a sensory disorder characterized by both paraesthesia and dysesthesia, encompassing numbness, tingling, shooting, burning, stabbing and throbbing pain and frequently dysfunctional motor function (da Costa et al., 2020; Tanay et al., 2017). These sensory symptoms point to a central role of the epidermal nociceptive system in CIPN pathophysiology (Zajackowska et al., 2019).

Paclitaxel stabilizes microtubules, thus inhibiting mitosis in proliferating cells (Xiao et al., 2006). In nociceptive neurons, however, interference with microtubule dynamics inhibits axonal transport affecting epidermal sensory fibre innervation (Smith et al., 2016; Zajackowska et al., 2019). Thus, paclitaxel produces an axonopathy that appears to underlie the sensory alterations suffered by cancer patients receiving the drug, including an increase of the electrical excitability of sensory fibres (Zhang & Dougherty, 2014). Higher neural excitability arises from an increase in the expression of **voltage-gated Na⁺** and **Ca²⁺ channels** and a decrease of **voltage-gated K⁺ ion channels** (Waxman & Zamponi, 2014). **TRP channels**, mitochondrial dysfunction and oxidative stress have been also involved (Zajackowska et al., 2019). Analytical studies of CIPN have used primary cultures of nociceptors obtained from rodents treated with paclitaxel following a range of regimes, from acute to chronic, to reproduce the thermal and mechanical hypersensitivity seen in humans (Hara et al., 2013; Smith et al., 2004). These studies suggested that paclitaxel also promoted the release of cytokines and chemokines from immune cells (Doyle et al., 2012; Son et al., 2019) that, in turn, sensitized nociceptors contributing to the CIPN sensory abnormalities (Zajackowska et al., 2019). Thus, the direct effect of paclitaxel on sensory neurons excitability remains poorly understood, as previous studies involved multifactorial components arising from the action of paclitaxel in different types of cells.

Primary cultures of DRG neurons have been proposed to preclinically model CIPN in vitro (Eldridge et al., 2020; Malgrange et al., 1994; Scuteri et al., 2006). Li et al. reported an in vitro model of nociceptors in culture that faithfully reproduced the acute toxicity of paclitaxel, including an increase in **pERK** and **pp38** expression along with an increment in the expression of algescic factors that resulted in an increase in the excitability of nociceptors (Li et al., 2020). In our present experiments, we have used a long-term, in vitro culture of DRG neurons (10 DIV) to investigate the time course of paclitaxel-induced sensitization of neural excitability after

What is already known

- Paclitaxel produces an axonopathy that appears to underlie the sensory alterations in chemotherapy-induced peripheral neuropathy.
- Paclitaxel promotes the release of cytokines and chemokines from immune cells that sensitize sensory neurons.

What this study adds

- Paclitaxel directly and reversibly increases IB4(–) and IB4(+) nociceptor excitability.
- Paclitaxel sensitization exhibits sex dimorphism as nociceptors from female rats are more sensitive.

What is the clinical significance

- Na_v1.8 and TRPV1 channels are key therapeutic targets for treating chemotherapy-induced peripheral neuropathy.
- Topical TRPV1 antagonists appear to be clinically useful therapeutics for alleviating chemotherapy-induced peripheral neuropathy symptomatology.

drug removal. We analysed the effect of paclitaxel on both IB4(–) and IB4(+) neural subpopulations, as well as in sensory neurons isolated from female and male rats, to evaluate the presence of any sexual dimorphism. We report that paclitaxel reversibly potentiated neural excitability, with a maximum at 48 h after drug treatment that had virtually dissipated 96 h post-treatment. Neural excitability resulted primarily in a decrease of the current rheobase in both neural populations. Molecularly, paclitaxel modulated Na⁺ and K⁺ currents that define AP waveform generation and the activity of **TRPV1** and **TRPM8** channels. Notably, we observed that DRG neurons from female rats seemed to be more sensitive to paclitaxel-evoked excitability than those derived from male rats. Taken together, our findings indicate a direct and reversible effect of paclitaxel on the excitability of IB4(–) and IB4(+) and a potential sex-related dimorphism on sensory neurons.

2 | METHODS

2.1 | Animals

All animal care and experimental procedures were approved by the Institutional Animal and Ethical Committee of the Miguel Hernández University of Elche (UMH.IDI.AFM.06.20) and the Autonomous Government of Valencia (2021/VSC/PEA/0089), in accordance with the guidelines of the Economic European Community in accordance to Directive 2010/63/EU, the National Institutes of Health, and the Committee for Research and Ethical Issues of the International Association for the Study of Pain. Animal studies are reported in compliance with the ARRIVE guidelines (Percie du Sert et al., 2020) and with the recommendations made by the *British Journal of Pharmacology* (Lilley et al., 2020). Most of the in vivo studies regarding the neurotoxic effects of paclitaxel have been previously performed on Wistar rats due to the similarities with the human pain pathway (Hara et al., 2013; Li et al., 2018). Therefore, our experiments were conducted on 12–20 weeks old male and female Wistar rats obtained from Servicio de Experimentación Animal (SEA) of Miguel Hernández University of Elche. Animals were housed in polycarbonate plastic cages (two to four animals per cage) at 21–23°C with a 12, h light/dark cycle in a controlled environment with water and food available ad libitum.

2.2 | Culture of DRG neurons

Rats under isoflurane anaesthesia (IsoFlo[®], Zoetis) were decapitated, and the vertebral column was excised. DRG were then isolated in a Petri dish containing Dulbecco's phosphate buffered saline (DPBS, Sigma-Aldrich) with the use of a stereo microscope (VWR). Thereafter, DRG neurons were isolated by incubating the ganglia with 0.25% (w/v) collagenase type IA (Sigma-Aldrich) in DMEM (Gibco) with 1% penicillin-streptomycin (P/S, 5000 U·ml⁻¹, Invitrogen) at 37°C for 1 h in 5% CO₂. After digestion, the DRG was mechanically dissociated by pipetting, placed into DMEM medium containing 10% of foetal bovine serum (FBS, Invitrogen) and 1% P/S and centrifuged at 300 x g at ≈22°C for 5 min. The supernatant with containing connective tissue was discarded and the cell pellet was resuspended. This centrifugation and resuspension procedure was performed 3 times. Cell culturing conditions were adapted from a previously described protocol (Newberry et al., 2016). One hour later, cell medium was replaced by Neurobasal-A medium (Gibco) supplemented with 1% P/S, B-27[®] Supplement (2%; Gibco) and GlutaMAX_{TM} (1%; Invitrogen). Nerve growth factor (NGF, 5 ng·ml⁻¹; Sigma-Aldrich), NaCl (5 mg·ml⁻¹; Sigma-Aldrich), uridine (17.5 μg·ml⁻¹; Sigma-Aldrich) and 5-fluoro-2-deoxyuridine (7.5 μg·ml⁻¹; Sigma-Aldrich) were added to the cell medium 24 h after seeding. For microelectrode arrays (MEA), due to technical requirements, the final NGF concentration was 100 ng·ml⁻¹. Cells were maintained at 37°C in a humidified incubator with 5% CO₂. During cell culture, half of the

medium was changed for fresh medium every 3–4 days. Five days after cell seeding, cells were treated with 1 μM of paclitaxel or with the vehicle (0.04% DMSO) for 24 h.

2.3 | Immunofluorescence staining

DRG neurons seeded in coverslips were washed with DPBS and fixed in 4% (v/v) paraformaldehyde (Sigma-Aldrich) for 20 min at room temperature. After three washes with DPBS, cells were permeabilized with 0.1% Triton X-100 (Sigma-Aldrich) for 5 min and blocked with 5% normal goat serum (NGS, Sigma-Aldrich) for 1 h at ≈22°C. Then, cells were incubated overnight at 4°C in DPBS solution with 5% NGS containing primary antibodies against the following targets: neuron-specific protein NeuN using a mouse monoclonal antibody at 1:50 dilution (Millipore, Cat# MAB377C3, RRID:AB_10918200); TRPV1 using a rabbit polyclonal antibody at 1:100 dilution (Alomone Labs, Cat# ACC-029, RRID:AB_2040258); TRPA1, with a rabbit polyclonal antibody, 1:100 (Alomone Labs, Cat# ACC-037, RRID:AB_2040232); TRPM8, with a rabbit polyclonal antibody, 1:100 (Alomone Labs, Cat# ACC-049, RRID:AB_2040254); Nav1.7, with a rabbit polyclonal antibody, 1:200 (Alomone Labs, Cat# ASC-008, RRID:AB_2040198); Nav1.8, with a rabbit polyclonal antibody, 1:200 (Alomone Labs, Cat# ASC-016, RRID:AB_2040188); and Nav1.9, with a rabbit polyclonal antibody 1:200 (Alomone Labs Cat# ASC-017, RRID:AB_2040200), respectively. The following day, cells were washed with DPBS and incubated with goat anti-rabbit IgG Alexa Fluor[®] 488, 1:500 (Thermo Fisher Scientific, Cat# A-11034, RRID:AB_2576217) and goat anti-mouse IgG Alexa Fluor[®] 568, 1:500 (Thermo Fisher Scientific, Cat# A-11031, RRID:AB_144696) secondary antibodies at ≈22°C for 1 h. After DPBS washed, cells were stained with DAPI, 300 nM (Thermo Fisher Scientific Cat# D1306, RRID:AB_2629482). Coverslips were mounted with Mowiol[®] (Calbiochem). All dilutions were freshly prepared the day of the experiment from original stocks stored in individual aliquots at –20°C. Samples were visualized with an inverted fluorescence microscope (Zeiss Axio Observer, Carl Zeiss). Fluorescence was quantified removing the mean background fluorescence from each cell fluorescence using Fiji[®] software (Fiji, RRID:SCR_002285) (Schindelin et al., 2012). Representative pictures shown were obtained with an inverted confocal microscope (Zeiss LSM 5 Pascal, Carl Zeiss). Experimental details of the immunocytochemical procedures conform with BJP guidelines.

2.4 | Patch-clamp recordings

Small-diameter (<30 μm) DRG neurons seeded in coverslips were registered in voltage and current-clamp modes. For cell culturing, crystals were coated with poly-L-lysine (50 μg·ml⁻¹, Sigma-Aldrich) for 2 h. After four washes with deionized water, crystals were incubated during 1 h at 37°C with laminin diluted in DMEM medium (10 μg·ml⁻¹; Sigma-Aldrich). After DRG neurons extraction,

laminin was replaced by the cell suspension diluted in DMEM 1% FBS 1% P/S. Patch pipettes from borosilicate glass with OD 1.5 mm × ID 1.17 mm (Warner Instruments) were pulled using a Flaming/Brown micropipette puller P-97 (Sutter Instruments) to have 2–5 MΩ resistance. Seal resistance was between 200 MΩ and 1.5 GΩ, and series resistance was compensated around 80%. Extracellular solution contained (in mM): 140 NaCl, 4 KCl, 2 CaCl₂, 2 MgCl₂, 10 HEPES, 5 glucose, 20 mannitol, pH 7.4 adjusted with NaOH. Pipette internal solution contained (in mM): 144 KCl, 2 MgCl₂, 10 HEPES, 5 EGTA, pH 7.2 adjusted with KOH. Experiments were performed in whole-cell configuration at ≈22°C. After establishing whole-cell access, cells were recorded in current-clamp mode. First, the resting membrane potential (RMP) was determined without any current injection. Cells with RMP higher than −40 mV or AP that did not overshoot 0 mV were not considered for analysis. Neurons that fired action potentials in the absence of stimulus were considered as having spontaneous activity (SA). To calculate the rheobase, the firing frequency and to classify neurons into tonic or phasic behaviour, 1 s current depolarizing pulses from 0 to 300 pA in 10 pA intervals were applied. The minimum current required to evoke the first action potential was considered as the current rheobase. Neurons were classified as phasic if they fired one or few action potentials at the onset of the current stimulus. Tonic neurons were those that were able to fire continuously during one or more of the 1 s current pulses. The AP parameters were measured in the action potential fired at the minimum current injected using 10 ms depolarizing pulses from 0 to 300 pA in 10 pA steps. AP threshold was considered when the upstroke slope was ≥10 V·s^{−1}. AP amplitude was measured from RMP to peak.

For voltage-clamp recordings, capacitive transients were compensated. Cells with capacitance values higher than 40 pF were excluded from the analysis. For measuring K⁺ currents, the fast-inactivating K⁺ current (K_A) and the non-inactivating K⁺ current remaining before the end of the protocol (K_{DR}), respectively, were measured in a 300 ms voltage-step protocol from −80 to 70 mV in 10-mV intervals. For registering Na⁺ currents, external solution contained (in mM): 70 NaCl, 65 choline chloride, 3 KCl, 1 CaCl₂, 1 MgCl₂, 20 TEA-Cl, CsCl₂ 10 HEPES and 10 glucose, pH 7.4 adjusted with NaOH. Pipette internal solution contained (in mM): 140 CsF, 10 NaCl, 1 EGTA, 5 glucose and 10 HEPES, pH 7.30 adjusted with CsOH. Na_v1.8 currents were isolated using previous described voltage steps protocols (Soriano et al., 2019). The G-V curves were calculated from current-voltage relations, using $G = I_x / (V - V_x)$, where I_x and V_x are the ionic currents and the equilibrium potential for Na⁺ or K⁺, respectively. These curves were fitted to Boltzmann equation and the voltage for half-maximum activation ($V_{1/2}$) and gating valence (z) were determined (details are given in figure legends).

Current responses to **capsaicin**, **allyl isothiocyanate (AITC)**, **menthol** and menthol with **AMTB** were measured using a continuous protocol at −60 mV. These compounds were applied diluted in external solution using a continuous perfusion system (10 ml·min^{−1}). To

activate TRPV1 and TRPA1 channels, four 1 μM capsaicin pulses of 15 s duration followed by a 60 s pulse of 100-μM AITC were applied, respectively. TRPM8 channel currents were elicited by a 20 s pulse of 100 μM menthol. Then, the TRPM8 channel blocker AMTB was used at 10 μM with menthol for 20 s. Data were acquired at 20 kHz for all the protocols except for the continuous voltage protocols performed to study capsaicin, AITC and menthol responses that were sampled at 1 kHz. These currents were additionally filtered to 2 Hz for plotting. Recordings were performed with an EPC10 amplifier controlled by Patchmaster software (HEKA Elektronik).

To study separately peptidergic and non-peptidergic DRG neurons, before each measurement, coverslips were incubated for 10 min with the fluorescent dye Isolectin-GS-IB4 Alexa Fluor[®] 568 conjugate (10 μg·ml^{−1}; Invitrogen) diluted in external solution, followed by two washes. As previously described, IB4 labelling did not alter viability or the electrophysiological parameters of the neurons (Stucky & Lewin, 1999). Cells were visualized with a fluorescent microscope (Axiovert 200 Inverted Microscope, Carl Zeiss) with an excitation filter ET545 and an emission filter ET605 (CHR-49004, Laser 2000 SAD). Cells that did not show fluorescence were considered as IB4(−). Only one cell per dish was recorded and analysed.

2.5 | Quantitative RT-PCR

Total RNA was isolated using the E.Z.N.A.[®] microElute total RNA kit (Omega Bio-tek). Extracellular RNA samples quantity and purity were analysed using the NanoDrop 1000 Spectrophotometer (ThermoFisher Scientific). Possible contaminating DNA was digested using the DNase I (Sigma), and then the RNA extracted was reverse transcribed using the First Strand cDNA Synthesis Kit (ThermoFisher Scientific). Primers targeting rat selective channels were designed, and their sequences were as follows: TRPV1: Fw: 5' TGGACGAGGTAAC TGGACT, Rv: AGTTTCTCCCTGAAACTCGG; TRPA1: Fw: 5' AGTGGC AATGTGGAGCGATA Rv: 5' TCCCGTCGATCTCAGCAATG; TRPM8: Fw: 5' GCTACGGACCAGCATTTCAT, Rv: 5' GCTTGTCATGGGCTT CTT; Na_v1.7: Fw: 5' TGGCGTCGTGTCGCTTGT, Rv: 5' TGGCCCTT GCCTGAGAT; Na_v1.8: Fw: 5' TCCTCTCACTGTTCCGCCTCAT, Rv: 5' TTGCTGCTCTGCTCTTCATAC; Na_v1.9: Fw: 5' ATACGGTGCCCT GATCCTCT, Rv: GGAAGTGAAGGGGCGGAAAT, Rpl29: Fw: 5' ACAG AAATGGCATCAAGAAACCC, Rv: 5' TCTTGTGTGCTTCTTGCAAAA. The complementary DNA (cDNA) was added to the PowerUp[™] SYBR[™] Green Master Mix (ThermoFisher Scientific) with the forward and reverse primers described and nuclease-free water. To verify the results, we used no template negative controls and reverse transcriptase minus (RT-) negative controls. Amplification and quantification of the cDNA was carried out with the QuantStudio3 Real-Time PCR Instrument (Applied Biosystems) using the following thermal cycling conditions: 50°C for 2 min, 90°C for 10 min; 40 cycles of 95°C during 15 s and 60°C for 1 min; and final steps of 95°C for 15 s, 60°C for 1 min and 95°C for 15 s. The expression level of the mRNA was normalized to the housekeeping Rpl29 mRNA levels and calculated using the 2^{−ΔΔCt} method.

2.6 | Immunoblotting

The immuno-related procedures used comply with the recommendations made by the *British Journal of Pharmacology* (Alexander et al., 2018). At DIV8, cell cultures were homogenized, dissolved in RIPA lysis buffer (50-mM HEPES, 140 mM NaCl, 10% glycerol, 1% v/v Triton X-100, 1 mM EDTA, 2 mM EGTA, 0.5% deoxycholate, pH 7.4) with EDTA-free protease inhibitor cocktail (cComplete™, Sigma-Aldrich) and centrifuged at 18400 × g at 4°C for 15 min. The supernatant was collected, and the protein concentration was determined using the Pierce™ BCA Protein Assay Kit (Thermo Scientific). Cellular protein extracts were mixed (1:1) with 2× sample buffer (0.125 mM Tris-HCl pH 6.8, 40 mg·ml⁻¹ SDS, 2 mg·ml⁻¹ bromophenol blue, 20% glycerol and 0.1-M dithiothreitol) boiled for 10 min. Thereafter, proteins were separated by electrophoresis on a 7.5% SDS-PAGE gel and transferred to a 0.45-µm nitrocellulose membrane (Bio-Rad) for 90 min at 100 V using an electrophoretic transfer system (Bio-Rad). Membranes were blocked with non-fat milk at 5% in TBST (200-mM glycine, 25 mM Tris base, 20% methanol and 0.05% Tween, pH 8.3) at room temperature for 1 h for all primary antibodies, except for TRPM8 that required 3-h blocking with non-fat milk and 0.5-h blocking with 5% BSA in TBST, according to manufacturer's instructions. Next, membranes were incubated at 4°C overnight with the following primary antibodies diluted in 1% BSA in TBST: rabbit anti-Actin, 1:1000 (Sigma-Aldrich, Cat# A2066, RRID:AB_476693); rabbit anti-TRPV1, 1:1000 (Alomone Labs, Cat# ACC-029); rabbit anti-TRPM8, 1:500 (Alomone Labs, Cat# ACC-049); rabbit anti-Na_v1.7, 1:2500 (Alomone Labs, Cat# ASC-008); and rabbit anti-Na_v1.8, 1:1000 (Alomone Labs, Cat# ASC-016), respectively. After washing the membranes with TBST, they were incubated with the secondary antibody anti-rabbit IgG, 1:20000 (Sigma-Aldrich, Cat# A0545, RRID:AB_257896). To minimize the number of animals used, blots were cut in three different sections to test the same blot with multiple antibodies. Signals were detected with the SuperSignal™ West Pico PLUS Chemiluminescent Substrate (Thermo Scientific), visualized in a ChemiDoc™ MP Imaging System (Bio Rad ChemiDoc MP Imaging System, RRID:SCR_019037) and quantified using Image Lab software (Image Lab Software, BioRad, RRID:SCR_014210). Protein signals were normalized to actin levels within the same blot.

2.7 | Data and statistical analysis

Data and statistical analysis comply with the recommendations on experimental design and analysis in pharmacology (Curtis et al., 2018), with the exceptions that data collection and analysis were not blinded because they were performed by the same researcher and, because effects and standard deviation could not be previously predicted, data were evaluated through experiments to minimize the number of animals used. Data were statistically analysed using the GraphPad Prism® 9.0.0 software (GraphPad

Prism, RRID:SCR_002798). For quantitative variables, first we assessed whether data followed a gaussian distribution using D'Agostino-Pearson (omnibus k2) normality test. Data with a normal distribution are expressed as mean ± SD and analysed with unpaired t tests as indicated. As the heterogeneity of DRG neurons is high, and our sample size was not sufficient to determine multiple associations, we restricted our statistical analysis to the defined groups (treatment and sex type) that were analysed using the two-way ANOVA test for parametric data, with the Tukey post hoc test when *F* achieved statistical significance or Kruskal–Wallis with Dunn's multiple comparisons test for non-parametric data.

Non-normal distribution data are expressed as median, (with Q25–Q75) and analysed with Mann–Whitney test. For qualitative variables, data are expressed as percentage and analysed with Fisher's exact test. Significant differences were set to *P* < 0.05.

For patch clamp experiments, *n* represents the number of cells measured and correspond to the number of independent experiments, as a single neuron was monitored in each vehicle and paclitaxel-treated crystal; *N* denotes the number of rats used. For immunofluorescence measurements, *n* represents the number of neurons, and *N* the number of independent experiments; and for MEA, *n* denotes the number of active electrodes. Statistical analysis was based on the number of independent experiments. Details of the statistics are reported in the figure legends or Supporting Information.

2.8 | Materials

Paclitaxel (Taxol®; Tocris Bioscience, Bristol, UK) was dissolved in DMSO to create a stock of 25 mM; these stock solutions were stored at –20°C and used within 1 month. Before cell treatment, the stock solution was diluted in DMEM 10% FBS 1% P/S and passed through a 0.2-µm filter. The required quantity was added to the cell medium to yield a final concentration of 1 µM. Controls were prepared following the same procedure using only DMSO (0.04%).

For electrophysiological experiments, capsaicin, AITC, menthol, AMTB and PF04885614 (all from Sigma, St. Louis, MO, USA) were dissolved in DMSO to have stock concentrations of 10 mM, 1 M, 1 M, 100 mM and 100 µM, respectively. ProTx II (Tocris Bioscience) stock solution was prepared in water to a concentration of 50 µM. The day of the experiment, these solutions were diluted in the external solution to reach the final concentration indicated for each experiment. Final concentration of DMSO was 0.01% of the total volume for capsaicin, AITC, menthol and AMTB, and 0.075% for PF04885614.

2.9 | Nomenclature of targets and ligands

Key protein targets and ligands in this article are hyperlinked to corresponding entries in <http://www.guidetopharmacology.org>, and are permanently archived in the Concise Guide to PHARMACOLOGY 2021/22 (Alexander et al., 2021).

3 | RESULTS

3.1 | Paclitaxel reversibly augmented the electrical excitability of small diameter DRG sensory neurons

The experimental paradigm consisted of seeding the sensory neurons (0 DIV) and, after their full maturation (5 DIV), treating them with 1 μ M paclitaxel for 24 h (Figure 1a). Thereafter, the drug was removed, and the neural excitability was evaluated at 0 (6 DIV), 48 (8 DIV) and

96 h (10 DIV) after paclitaxel removal (post-treatment) (Figure 1a). As control, DRG cultures were exposed to paclitaxel vehicle (0.04% DMSO). We used 1 μ M paclitaxel as a clinically relevant concentration (C_{max}) reached in a 24h infusion (Ohtsu et al., 1995). Incubation of neural cultures with paclitaxel for 24 h did not affect cell viability as neurons display normal RMPs, although it produced an axonal retraction (Figure 1b).

Paclitaxel increased the excitability of small diameter sensory neurons in a time-dependent manner, as shown by the larger number

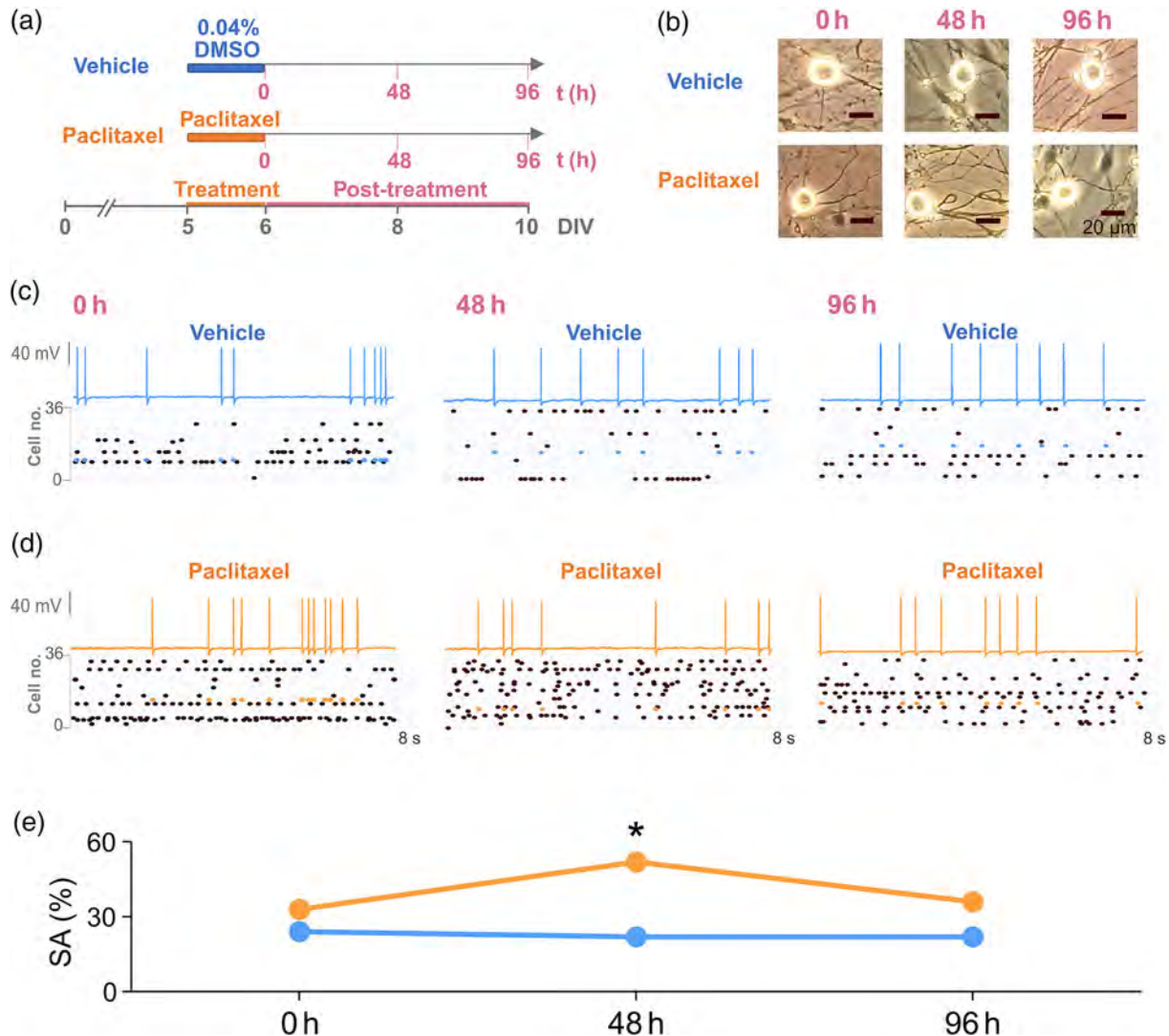


FIGURE 1 Small DRG neurons displayed increased excitability 48 h after paclitaxel treatment. (a) Diagram of the experimental design used for investigating the effect of paclitaxel on DRG neurons activity. Cells were incubated with the vehicle (0.04% DMSO) or with 1 μ M paclitaxel during 24 h between days 5 and 6 of culture (5–6 DIV). Electrical recordings were performed at 0 h (DIV6), 48 h (DIV8) and 96 h (DIV10) post-treatment. (b) Representative images of the DRG neurons through the culture after paclitaxel exposure (lower panels) in comparison with vehicle condition (upper panels). (c and d) Representative recordings (top) and raster plot (bottom) of DRG neurons spontaneous firing of APs at 0, 48 and 96 h after vehicle (c) or paclitaxel (d) exposure. Each dot represents an individual spike fired during an 8 s protocol at 0 pA of current. The cell corresponding to the AP recording shown is blue coloured for vehicle and orange for paclitaxel-treated neurons in the raster plots. (e) Percentage of small DRG neurons exhibiting spontaneous activity (SA) at 0, 48 and 96 h after vehicle or paclitaxel treatment. Data are given as percentage with $N = 15$, $n = 34$ for vehicle and $n = 54$ for paclitaxel 24 h after exposure; $N = 20$, $n = 46$ for vehicle and $n = 54$ for paclitaxel, 48 h after exposure; $N = 19$, $n = 50$, 96 h after exposure. Results are shown as individual values with means \pm SEM. * $P < 0.05$, significantly different from vehicle; Fisher's exact test

of sensory neurons exhibiting SA (Figure 1c,d, Table S1), that increased 2.4-fold at 48 h post-treatment and declined to virtually normal levels at 96 h (Figure 1e). We also observed a 1.8-fold increase in the percentage of small diameter sensory neurons exhibiting tonic firing, along with a 2-fold decrease in their current rheobase (Table S1). Thus, paclitaxel reversibly increased electrogenicity of sensory neurons, peaking at 48 h post-treatment and virtually dissipating at 96 h.

3.2 | Paclitaxel increased electrical firing in IB4(−) and IB4(+) sensory neurons

We next investigated the effect of paclitaxel on the electrical excitability of IB4(−) and IB4(+) neurons. In both neural populations, we observed a similar reversible effect of paclitaxel on their electrical activity, peaking at 48 h post-treatment (Tables S2 and S3). Paclitaxel increased the percentage of IB4(−) neurons displaying SA (Figure 2a) without changing the SA mean firing frequency (Figure 2c, Table S2). The chemotherapeutic drug significantly depolarized the RMP of IB4(−) nociceptors (Figure 2d). Similarly, IB4(+) neurons revealed a strong increase in the percentage of neurons exhibiting SA after paclitaxel exposure (Figure 2b,c, Table S3). We observed a tendency to RMP depolarization, but it did not reach statistical significance (Figure 2d). Cell capacitance and input resistance were not altered by paclitaxel in either neural population (Figure 2e,f).

We also evaluated paclitaxel effect on electrically evoked AP firing in both neural subtypes (Figure 3). As shown in Figure 3a, 55% of IB4(−) neurons recorded 48 h post-treatment exhibited tonic AP firing in

response to a 120 pA current pulse (Table S2). Notably, paclitaxel augmented the firing frequency 2-fold (Figure 3a,b; Table S2) and significantly reduced the current rheobase (Figure 3b,e,f; Table S2). Notice that this increment in firing frequency was observed in the full range of currents from 10 to 300 pA (Figure 3b, Table S2), which resulted in an increment in the percentage of IB4(−) neurons exhibiting tonic firing (Figure 3g; Table S2). IB4(+) neurons primarily exhibited phasic AP firing when stimulated with a 120 pA current pulse. Paclitaxel increased 3-fold AP triggering (Figure 3c,d, Table S3), concomitant to a 3-fold decrease in the current rheobase, resulting in a 2-fold increment in the percentage of IB4(+) neurons exhibiting repetitive AP discharging after drug treatment (Figure 3g). These changes in the current rheobase and the percentage of IB4(+) neurons firing tonically disappeared 96 h after paclitaxel exposure (Table S3). Therefore, paclitaxel treatment of DRG cultures increased the electrogenic activity of both IB4(−) and IB4(+) neural subtypes. The effect on IB4(+) neurons is notable as they change from a silent and phasic to a tonic firing phenotype.

3.3 | Paclitaxel altered the electrical properties of IB4(−) and IB4(+) action potentials

The decrease in the current rheobase and the increase in repetitive firing in both IB4(−) and IB4(+) neurons produced by paclitaxel suggest an alteration in the AP waveform (Figure 4a). In control conditions, we observed that 58% of IB4(−) neurons exhibited a typical AP waveform with an inflection in the AP repolarization phase. Paclitaxel reduced this percentage to 27% of neurons. Paclitaxel also reduced the amplitude and accelerated the AHP phase. The t_r and the t_{AHP} were 32% and 22%

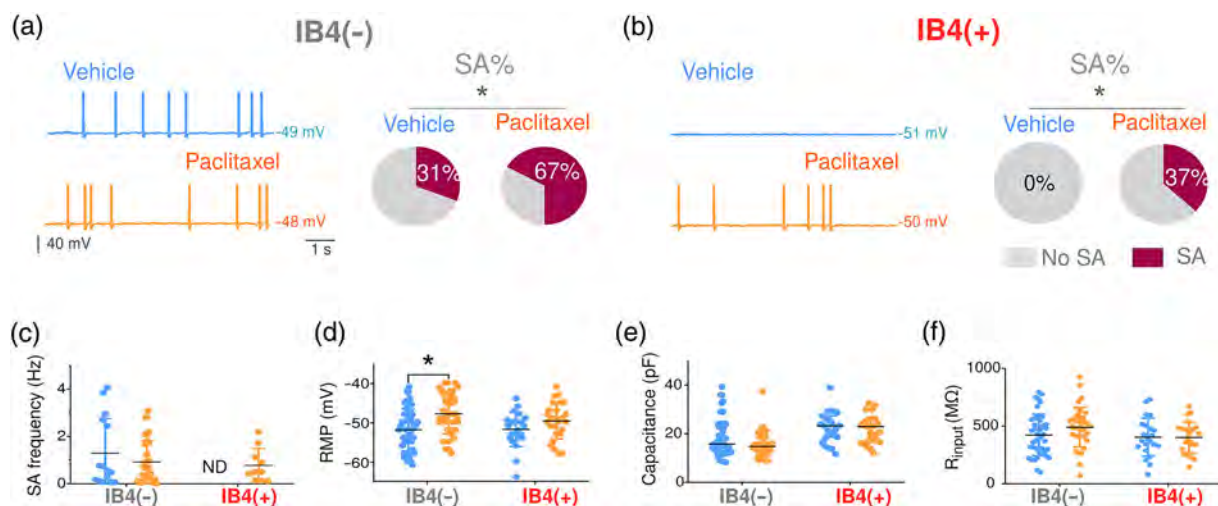


FIGURE 2 Paclitaxel increased the number of IB4(−) and IB4(+) neurons displaying spontaneous activity. (a and b) Representative AP recordings of IB4(−) (a) and IB4(+) (b) neurons 48 h after vehicle or paclitaxel treatment fired spontaneously (0 pA). The percentage of neurons firing SA for each group is indicated on the right as pie charts. The SA (%) is indicated inside the chart. (c) Frequency of spontaneous AP firing in 30 s recordings. Spontaneous activity was not detected in IB4(+) neurons treated with vehicle (ND). (d) Resting membrane potential (RMP) for IB4(−) and IB4(+) neurons at 48 h after vehicle or paclitaxel treatment. (e) Capacitance of the cells recorded in vehicle and paclitaxel groups for IB4(−) and IB4(+) neurons was not statistically different. (f) Input resistance (R_{input}) remains unaltered for IB4(−) and IB4(+) neurons after paclitaxel exposure. Results are shown as individual values with means \pm SD. $N = 20$, for IB4(−) with $n = 49$ for vehicle and $n = 42$ for paclitaxel; $N = 13$, for IB4(+) with $n = 25$. * $P < 0.05$, significantly different from vehicle; Fisher's exact test (a and b), unpaired t test (c, d and f) or Mann-Whitney test (e)

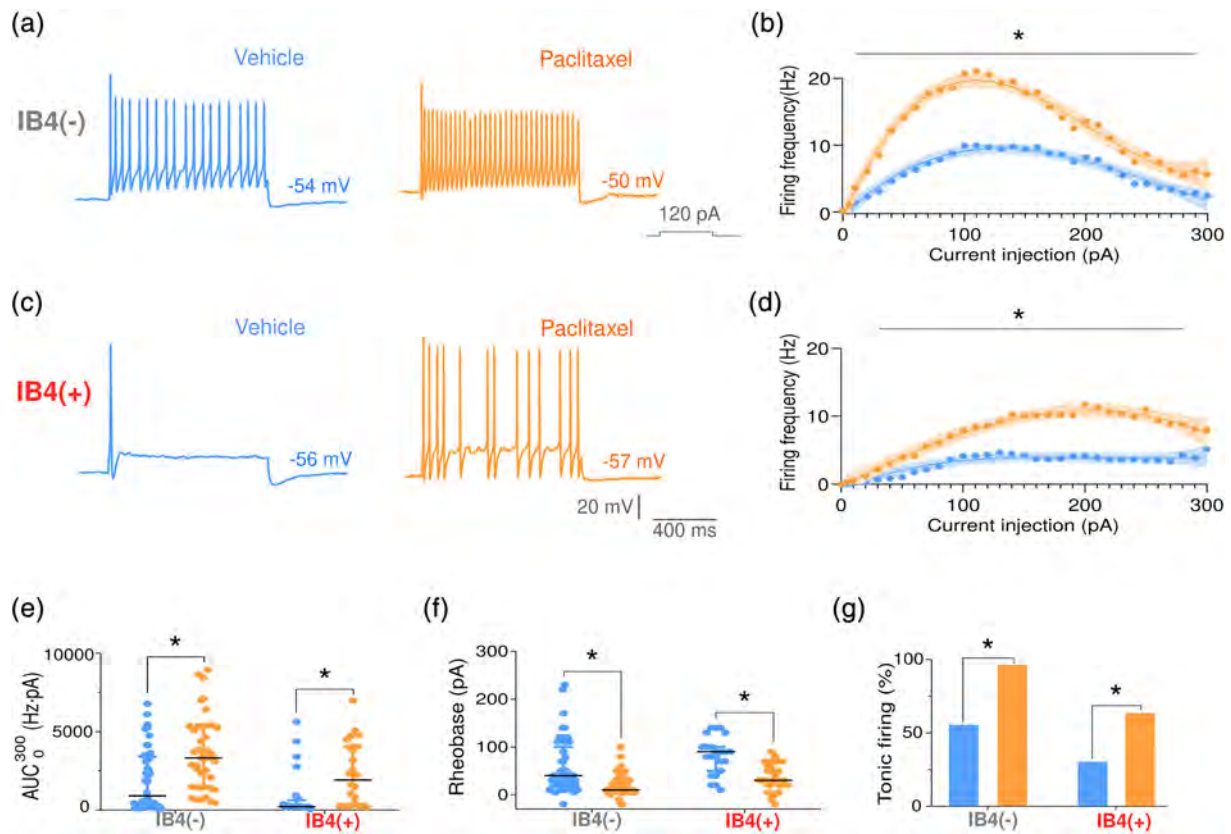


FIGURE 3 Paclitaxel potentiated electrically-evoked AP firing of IB4(-) and IB4(+) small-DRG neurons. (a and c) Representative recordings of AP firing evoked by a 1 s of current injection pulse of 120 pA for IB4(-) (a) and IB4(+) (c) neurons exposed to vehicle or paclitaxel recorded 48 h post-treatment. (b and d) Firing frequency (no. of APs evoked during 1 s depolarizing pulse) at each current injected from 0 to 300 pA in 10-pA intervals for IB4(-) (b) and IB4(+) (d) neurons exposed to vehicle or paclitaxel. (e) Area under the curve (AUC_{0-300}) obtained plotting the firing frequency as a function of the injected current in the range of 0 to 300 pA. (f) Rheobase values for IB4(-) and IB4(+) small DRG neurons exposed to vehicle or paclitaxel. (g) Percentage of neurons exposed to vehicle and paclitaxel exhibiting tonic firing. Data are expressed as individual values with medians, with interquartile ranges (IQR). Each dot represents the values measured for each cell recorded. Data were collected 48 h post-treatment. $N = 20$, for IB4(-) with $n = 49$ for vehicle and $n = 42$ for paclitaxel; $N = 13$, for IB4(+) with $n = 25$. * $P < 0.05$, significantly different from vehicle; Mann-Whitney test (b, d, e and f) or Fisher's exact test (g)

faster in drug treated IB4(-) neurons (Figure 4b). In addition, the AHP amplitude in these neurons was significantly reduced by 3 mV (Figure 4c). Other AP properties such as the t_{peak} , the V_{th} , overshoot, amplitude and the maximum upstroke slope were not altered by paclitaxel (Figure 4b-e). A similar analysis in IB4(+) neurons revealed that paclitaxel significantly depolarized the AHP amplitude by 3 mV (Figure 4h). All the other parameters did not evidence a statistically significant difference (Figure 4g-j). Thus, the higher electrical excitability observed in paclitaxel-treated IB4(-) and IB4(+) neurons appears primarily to arise from a smaller AHP and, in IB4(-) neurons, a faster repolarization and AHP recovery were also contributors.

3.4 | Paclitaxel increased Na_v channel currents in IB4(-) and IB4(+) neurons

IB4(-) sensory neurons displayed fast-inactivating inward currents upon 40 ms depolarizing pulses (Figure 5a), with a typical J-V curve

for Na^+ ionic currents. The G-V relationship (Figure 5b) showed that paclitaxel hyperpolarized the $V_{1/2}$ and slightly altered the total Na^+ inward current, without altering the recovery from inactivation (Figure 5c). In contrast, paclitaxel did not affect the J-V nor the G-V curves of IB4(+) neurons (Figure 5d,e) but promoted a faster recovery of their Na^+ currents from inactivation (Figure 5f).

Because $Na_v1.7$ and $Na_v1.8$ channels have been shown to be altered by paclitaxel in animal models (Li et al., 2018; Zhang et al., 2018), we evaluated if the chemotherapeutic drug also affected them in our pre-clinical model. We used ProTx II and PF04885614 as specific blockers of $Na_v1.7$ and $Na_v1.8$ channels to study the contribution of these channels to Na^+ currents in IB4(-) and IB4(+) neurons (Figure 6). $Na_v1.7$ and $Na_v1.8$ ionic currents were obtained by subtracting the Na^+ ionic currents recorded in the presence of the blockers from that in their absence (Figure S1). In IB4(-) neurons, paclitaxel did not significantly alter $Na_v1.7$ currents (Figure 6a). A similar result was observed in IB4(+) neurons (Figure 6b). For $Na_v1.8$ channels, we observed an apparent current increase in IB4(+) nociceptors

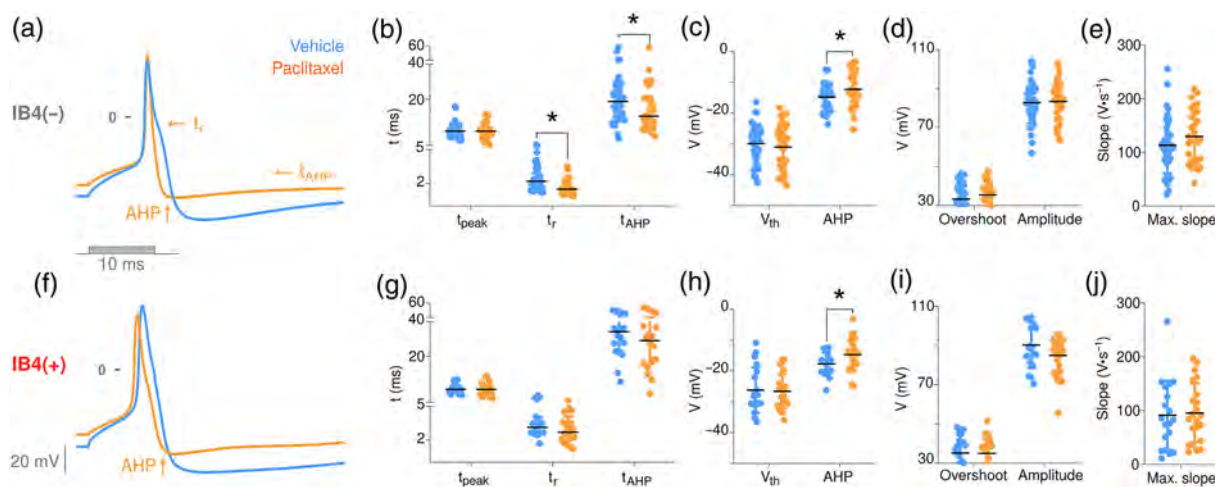


FIGURE 4 Paclitaxel altered the action potential parameters of IB4(-) and IB4(+) neurons. (a and f) Representative APs of IB4(-) (a) and IB4(+) (f) neurons exposed to vehicle or paclitaxel. Arrows mark action potential parameters in which statistical differences were found, as the repolarization time (t_r), the AHP amplitude (AHP) and the duration of the half AHP (t_{AHP}). APs were triggered using 10 ms current pulses from 0 to 300 pA and analysed at the current threshold. (b and g) Time to peak (t_{peak}), t_r and t_{AHP} parameters for IB4(-) (b) and IB4(+) neurons (g). t_r and t_{AHP} were significantly shorter in paclitaxel-treated IB4(-) neurons, whereas in IB4(+) neurons, there were no significant changes in t_r , t_{peak} and t_{AHP} , following paclitaxel. (c and h) Action potential threshold (V_{th}) and AHP recorded for IB4(-) (c) and IB4(+) (h) neurons. Although the V_{th} was not affected by paclitaxel treatment in either set of neurons, the AHP amplitude was significantly increased by paclitaxel in both IB4(-) and IB4(+) neurons. (d and i) Overshoot and amplitude for IB4(-) (d) and IB4(+) (i). These parameters were not affected by paclitaxel treatment in either set of neurons. (e and j) Maximum upstroke slope (max. slope) for IB4(-) (e) and IB4(+) (j) neurons. This parameter was not affected by paclitaxel treatment in either set of neurons. Data were collected 48 h post-treatment. Values are expressed as mean \pm SD. $N = 20$, $n = 37$ for vehicle, $n = 34$ for paclitaxel treated IB4(-) cells; $N = 10$, $n = 19$ for vehicle, $n = 22$ for paclitaxel IB4(+) cells. * $P < 0.05$, significantly different as indicated; unpaired t test or Mann-Whitney test (for t_{AHP} for IB4(-) and t_r for IB4(-) and IB4(+) cells)

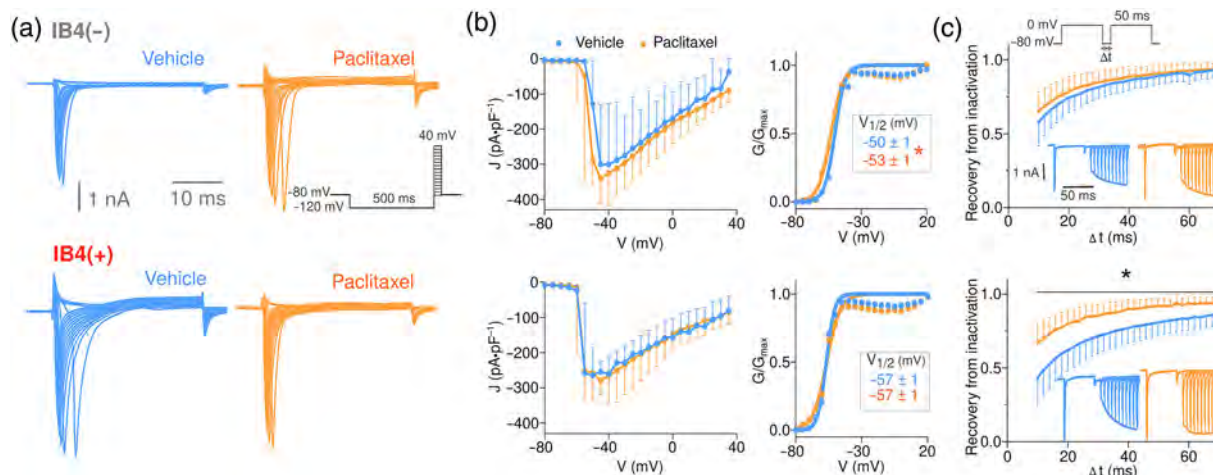


FIGURE 5 Na_v channel activity after exposure of IB4(-) and IB4(+) neurons to vehicle or paclitaxel. (a) Representative recordings of a family of ionic currents evoked using the 30 ms depolarizing protocol from -80 mV to 35 mV in 5 mV steps for IB4(-) and IB4(+) neurons 48 h after vehicle or paclitaxel treatment for IB4(-) (up) and IB4(+) (down) neurons. (b) J-V relationships of Na^+ inward currents present in the recordings for IB4(-) (up) and IB4(+) (down). J ($pA \cdot pF^{-1}$) median values (with interquartile range) are shown. Right G-V curves obtained from the J-V curves. Reversal potential was interpolated from each J-V curve. Curves were fitted to the Boltzmann equation: $G/G_{max} = \left(1 / \left(1 + e^{-\frac{zF(V_{1/2}-V)}{RT}}\right)\right)$.

(c) Recovery from inactivation of the Na_v currents against time for IB4(-) (up) and IB4(+) (down). Representative registers of the Na_v recovery from inactivation are indicated in each graph. Data are expressed as medians (with interquartile range). Data were collected 48 h post-treatment. IB4(-): $N = 5$, $n = 18$ for vehicle and $n = 19$ for paclitaxel; IB4(+): $N = 5$, $n = 16$ for vehicle and $n = 18$ for paclitaxel. * $P < 0.05$, significantly different from vehicle; Mann-Whitney test for J, unpaired t test for recovery from inactivation

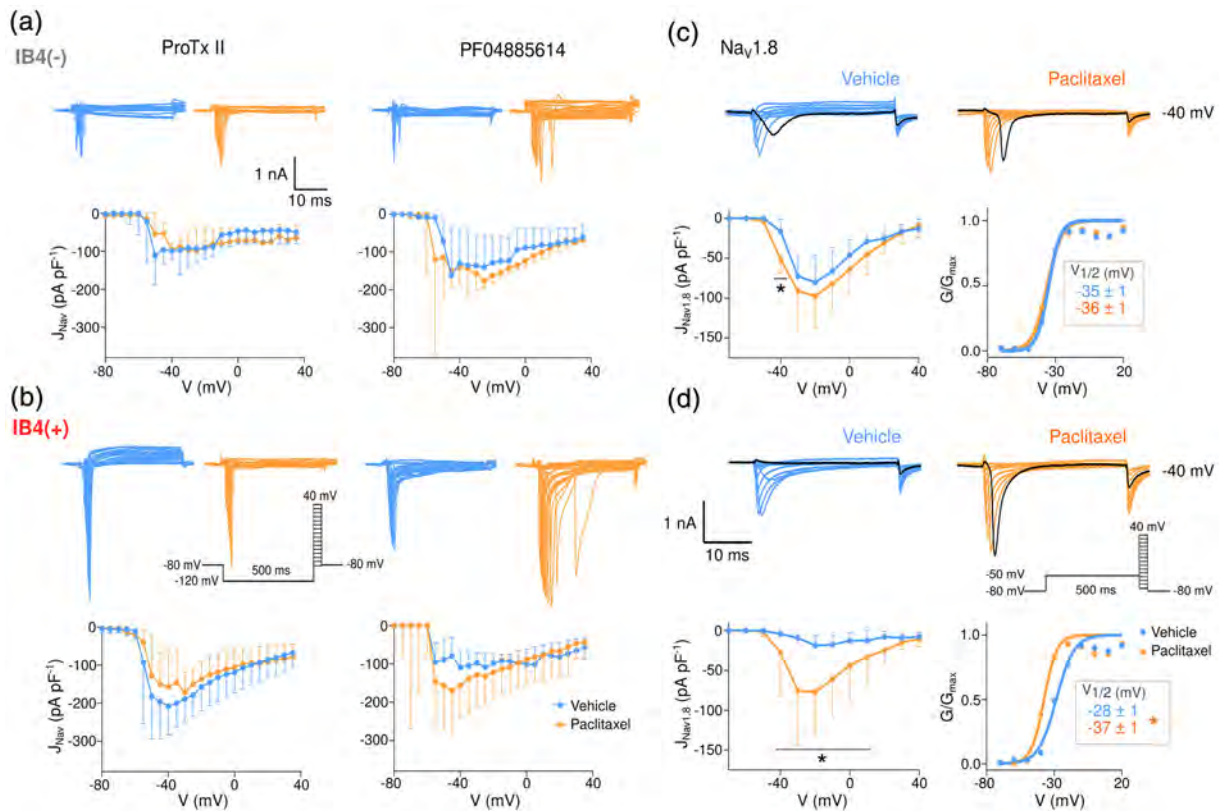


FIGURE 6 Paclitaxel augmented $\text{Na}_v1.8$ currents in IB4(−) and IB4(+) sensory neurons. (a and b) Pharmacological dissection of vehicle and paclitaxel Na_v currents using the specific blockers: ProTx II at 10 nM for $\text{Na}_v1.7$ channels and PF04885614 at 75 nM for $\text{Na}_v1.8$ channels. The current after blockade was subtracted from the total current measured. J - V relationships of Na^+ inward currents for each channel indicated below their respective representative registers for IB4(−) (a) and IB4(+) (b). J ($\text{pA}\cdot\text{pF}^{-1}$) median values (with interquartile range) are shown. $N = 5$, $n = 6$ for each blocker. (c and d) Representative registers of the isolated $\text{Na}_v1.8$ currents activated using a voltage protocol from -70 to 40 mV in 10 mV intervals. Black lines indicate the ionic current detected at -40 mV for IB4(−) (c) and IB4(+) (d). JV and GV curves for $\text{Na}_v1.8$ current are exhibited below the recordings. $V_{1/2}$ values are indicated inside squares. Data are expressed as medians (with interquartile range). Data were collected 48 h post-treatment. $N = 7$. IB4(−): $n = 17$ for vehicle, $n = 19$ for paclitaxel; IB4(+): $n = 17$ for vehicle, $n = 21$ for paclitaxel. $*P < 0.05$, significantly different from vehicle; Mann-Whitney test for J and the unpaired t test for $V_{1/2}$

(Figure 6b) that was less evident in IB4(−) sensory neurons (Figure 6a). To further interrogate the potential alteration of $\text{Na}_v1.8$ currents, we applied a stimulation protocol consisting in a 500-ms depolarizing pre-pulse to -50 mV to inactivate TTX-sensitive and TTX-resistant Na_v channels, followed by a family of 30-ms depolarizing 10 mV step potentials from -70 mV to 40 mV to monitor the activity of $\text{Na}_v1.8$ channels (Figure 6c,d) (Soriano et al., 2019). In IB4(−) neurons, paclitaxel produced a modest increase in $\text{Na}_v1.8$ ionic currents (Figure 6c). In contrast, paclitaxel produced a significant increase in $\text{Na}_v1.8$ ionic currents in IB4(+) neurons (Figure 6d) that was accompanied by a 9 mV hyperpolarizing shift of the $V_{1/2}$ (Figure 6d). Furthermore, treatment of IB4(+) neurons with PF04885614 inhibited the fast recovery from inactivation promoted by paclitaxel (Figure S2). To substantiate these findings, we evaluated the expression of these channels. mRNA levels of $\text{Na}_v1.7$, $\text{Na}_v1.8$ and $\text{Na}_v1.9$ in nociceptor cultures were not significantly affected by paclitaxel (Table S5). Similarly, we did not detect a significant increase in the protein expression in whole cell extracts evaluated by immunoblotting (Figure S3). However, immunocytochemical measurements

revealed a significant increase in $\text{Na}_v1.8$ immunoreactivity in sensory neurons treated with paclitaxel consistent with an increment in protein expression in a subset of neurons (Figure S4). Taken together, these results imply that in our in vitro nociceptor model paclitaxel primarily appears to increase the expression and function of $\text{Na}_v1.8$ channels.

3.5 | Paclitaxel affected A-type K^+ currents in IB4(−) and IB4(+) DRG neurons

We also studied the effect of paclitaxel on K^+ currents in IB4(−) and IB4(+) neurons. In IB4(−) neurons, depolarizing 10 -mV voltage pulses from -80 to 40 mV evoked a family of outwardly rectifying, non-inactivating K^+ currents (K_{DR}). Paclitaxel produced outwardly rectifying K^+ currents that displayed two discernible components, a fast-inactivating A-type current (K_{A}) followed by a K_{DR} current, clearly shown at depolarizing potentials ≥ -30 mV (Figure 7a). Their distinct kinetics allowed us to analyse both K^+ currents (McFarlane & Cooper, 1991). The J - V

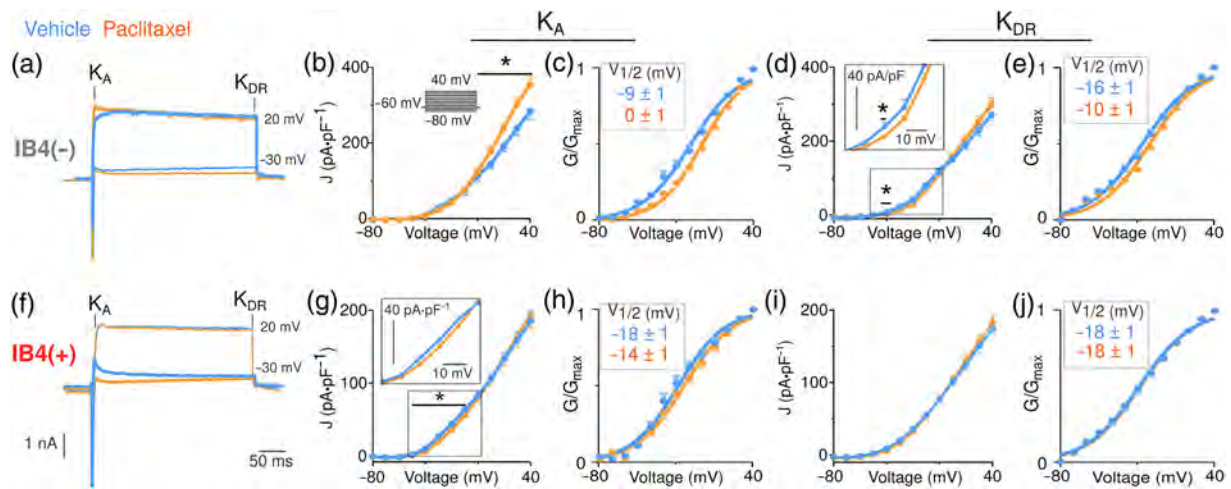


FIGURE 7 Paclitaxel affected the fast-inactivating (K_A) component of K^+ outward currents in IB4(-) and IB4(+) neurons. (a and f) Representative recordings of ionic currents in response to a depolarizing pulse to 20 mV and -30 mV for IB4(-) (a) and IB4(+) (f) neurons. Note that a fast-inactivating (K_A) and non-inactivating (K_{DR}) components can be distinguished. (b, d, g and i) J-V relationships of K_A and K_{DR} components in IB4(-) (b and d) and IB4(+) (g and i). Current densities ($\text{pA}\cdot\text{pF}^{-1}$) are given as median values with interquartile range. (c, e, h and j) G-V curves obtained from IV curves for K_A and K_{DR} for IB4(-) (c and e) and IB4(+) (h and j) using a $V_{K^+} = -92$ mV. Mean values with SEM are shown and curves were fitted to Boltzmann equation (see Figure 5 legend) with the following parameters: for IB4(-) K_A (c): Vehicle: $z = 1.4 e_0$, $df = 546$, $R^2 = 0.85$; paclitaxel: $z = 1.5 e_0$, $df = 440$, $R^2 = 0.9$; for K_{DR} (e): Vehicle: $z = 1.3 e_0$, $df = 559$, $R^2 = 0.9$; paclitaxel: $z = 1.3 e_0$, $df = 557$, $R^2 = 0.9$; for IB4(+) K_A (h): Vehicle: $z = 1.4 e_0$, $df = 258$, $R^2 = 0.9$; paclitaxel: $z = 1.4 e_0$, $df = 348$, $R^2 = 0.9$; for K_{DR} (j): Vehicle: $z = 1.3 e_0$, $df = 245$, $R^2 = 0.9$; paclitaxel: $z = 1.3 e_0$, $df = 349$, $R^2 = 1.0$ half-maximum activation voltages ($V_{1/2}$) for each G-V curve are indicated inside a square on each graph. Data were collected 48 h post-treatment. IB4(-): $N = 15$, $n = 28$ for vehicle and $n = 33$ for paclitaxel. IB4(+): $N = 13$, $n = 20$ for vehicle, $n = 27$ for paclitaxel. * $P < 0.05$, significantly different from vehicle; Mann-Whitney test

relationship for K_A currents showed that paclitaxel significantly increased the magnitude of this component at $V \geq 10$ mV (Figure 7b). Paclitaxel effect on K_A currents could be larger as it may be partially obscured by the presence of the K_{DR} currents. The G-V curve was shifted to depolarizing potentials, resulting in a 9 mV right-shift of the $V_{1/2}$ (Figure 7c). In contrast, the magnitude of K_{DR} currents was not significantly affected by paclitaxel (Figure 7d), whereas the G-V curve appeared depolarized by 6 mV, most likely because of the change in the K_A current.

In IB4(+) neurons, depolarizing voltage pulses elicited both K_A and K_{DR} currents (Figure 7f). Paclitaxel reduced 20% the K_A current magnitude (Figure 7g,i) but did not alter the $V_{1/2}$ (Figure 7h,j). Therefore, the drug promoted the appearance of a high threshold K_A current in IB4(-) neurons, while in IB4(+) neurons, it reduced a low threshold K_A current.

3.6 | Paclitaxel sensitized IB4(-) and IB4(+) neurons from both female and male rats

Next, we evaluated whether there was any sign of sex dimorphism in the neural sensitization by paclitaxel (Figure 8). Paclitaxel augmented 2-fold the percentage of IB4(-) neurons of both sexes exhibiting SA (Table S4), as well as their tonic firing (Figure 8a,b). Paclitaxel intensified the firing activity of female IB4(-) neurons by 2.2-fold, while for male neurons there was a 1.5-fold increase. The peak of the bell-shaped curve in female neurons was shifted towards lower current values (Figure 8c), implying a stronger sensitizing effect in female IB4

(-) neurons (Figure 8g, Table S4). Furthermore, paclitaxel significantly reduced the current rheobase in female IB4(-) neurons (Figure 8h, Table S4) and depolarized the RMP by 4 mV (Figure 8i, Table S4). In male IB4(-) neurons, the effect of paclitaxel on the current rheobase and RMP did not reach statistical significance.

In IB4(+) neurons, paclitaxel increased the percentage of neurons displaying SA in both sexes, by up to 40% (Table S4). Noteworthy, the drug increased ≥ 3.0 -fold tonic firing in female IB4(+) neurons and 1.5-fold in male (Figure 8d,g). This augment of AP firing in female IB4(+) neurons was also accompanied by a 3-fold decrease of the current rheobase (Figure 8h, Table S4). The drug also depolarized the RMP of female IB4(+) neurons as compared to male neurons, although it did not reach statistical significance (Figure 8i, Table S4). Thus, small sensory neurons from female rats appear more sensitive to paclitaxel potentiation than those from males.

3.7 | Paclitaxel increased TRPV1 and TRPM8 channel functionality

TRPV1, TRPM8 and TRPA1 are thermoTRP channels that may be implicated in the thermal hypersensitivity experienced by CIPN patients (Nazıroğlu & Braidı, 2017). Multielectrode array measurements revealed that paclitaxel augmented by ≥ 3 -fold the electrogenic responses to capsaicin or menthol, without altering TRPA1 channel activity (Figure S5), suggesting an increment in the expression of TRPV1 and TRPM8 channels. However, analysis of their mRNA

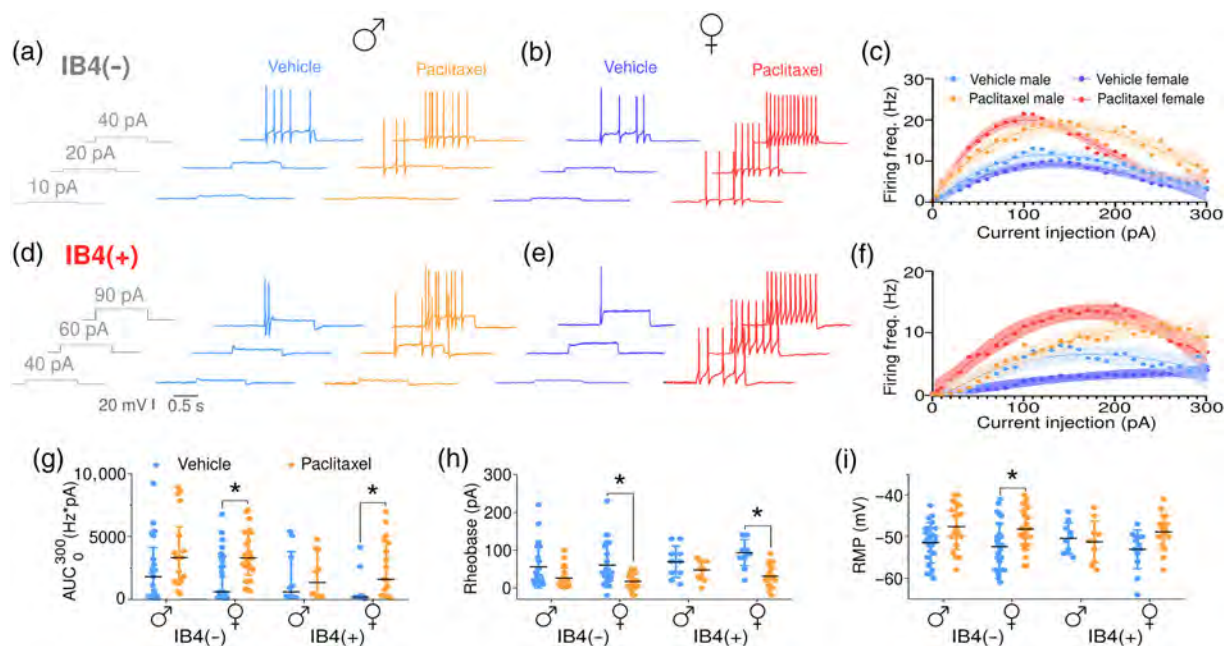


FIGURE 8 Neural excitability of IB4(-) and IB4(+) neurons from female rats appear more sensitive to paclitaxel. (a, b, d and e) Representative action potential firing of IB4(-) and IB4(+) neurons from female (b and e) and male (a and d) rats evoked by 1 s current pulse as indicated on the left side. (c and f) Firing frequency as a function of the injected current in the range of 0 to 300 pA in 10-pA pulses. Firing frequency was obtained counting the number fired APs during the 1 s current pulse. (g) Area under the curve (AUC₀₋₃₀₀) obtained by integrating the firing frequency curve for the 0 to 300 pA current interval in female and male neurons. (h) Rheobase values estimated as the minimum injected current need to fire an action potential in female and male neurons. (i) RMP measured using a continuous current protocol of 0 pA in female and male neurons. Data are presented as individual values and the means ± SD. Data were collected 48 h post-treatment. Male IB4(-): *N* = 9, vehicle: *n* = 23, paclitaxel: *n* = 19; female IB4(-): *N* = 11, vehicle: *n* = 26, paclitaxel: *n* = 23; male IB4(+): vehicle: *n* = 10, paclitaxel: *n* = 10; female IB4(+): vehicle: *n* = 13, paclitaxel: *n* = 17. IB4(-) and IB4(+) neurons were analysed separately. **P* < 0.05, significantly different as indicated; Kruskal-Wallis test with Dunn's multiple comparisons test (g, h) or two-way ANOVA with Tukey's multiple comparisons test (i)

expression (Table S5) did not show a transcriptional regulation by paclitaxel of these channels. At a protein level, we observed a significant increase of TRPV1 expression (Figure S3). Similarly, immunocytochemical analysis of sensory neurons revealed a significant increase of TRPV1 immunoreactivity (Figure 9b,c). For TRPM8, we observed an increase in immunoreactivity (Figure 9h,i) that was not substantiated by immunoblots (Figure S3). TRPA1 immunoreactivity was not affected by paclitaxel (Figure 9e,f).

We next evaluated the effect of paclitaxel on the ionic currents induced by capsaicin, menthol and AITC in IB4(-) and IB4(+) neurons (Figure 10; Table S6). Figure 10A illustrates representative capsaicin inward currents elicited in IB4(-) and IB4(+) neurons exposed to vehicle and paclitaxel. Capsaicin-evoked ionic currents were 4-fold augmented in IB4(-) neurons and mildly promoted in IB4(+) neurons treated with the drug (Figure 10B). As expected, paclitaxel did not affect the AITC-evoked ionic currents in either neural population (Figure 10c,d). In contrast, paclitaxel increased 3-fold the menthol response in IB4(-) neurons (Figure 10e,f). No menthol currents were recorded from IB4(+) neurons. Thus, these results indicate that paclitaxel mainly increased TRPV1 and TRPM8 channel activity in IB4(-) neurons.

We also investigated if paclitaxel potentiation of TRPV1 and TRPM8 activity displayed sexual dimorphism. Paclitaxel similarly

increased capsaicin-evoked ionic currents in male and female IB4(-) neurons by ≥ 3.5 -fold (Figure 10g,h). In contrast to the effects obtained with capsaicin, paclitaxel augmented menthol-evoked ionic currents 4.5-fold in male IB4(-) neurons but showed no significant increase in female IB4(-) neurons (Figure 10i,j). Paclitaxel similarly affected the capsaicin currents of IB4(+) male and female neurons (Figure 10k,l). Accordingly, paclitaxel similarly potentiated capsaicin responses in male and female sensory neurons, but the responses to menthol were potentiated only in male IB4(-) neurons.

4 | DISCUSSION

We have examined the direct effect of paclitaxel on nociceptor excitability using a long-term, in vitro, pre-clinical model of nociception that allowed us to study the reversibility of paclitaxel-induced neural sensitization. A salient finding was that paclitaxel exposure (24 h) increased SA and tonic firing of IB4(-) and IB4(+) sensory neurons, peaking at 48 h and dissipating at 96 h post-treatment. Potentiation of the electrogenic activity mainly resulted from a reduction of the current rheobase in IB4(-) and IB4(+) neurons, and a modest RMP depolarization in IB4(-) neurons. IB4(+) neurons shifted from a phasic to an irregular tonic firing, while in IB4(-) neurons, the tonic firing

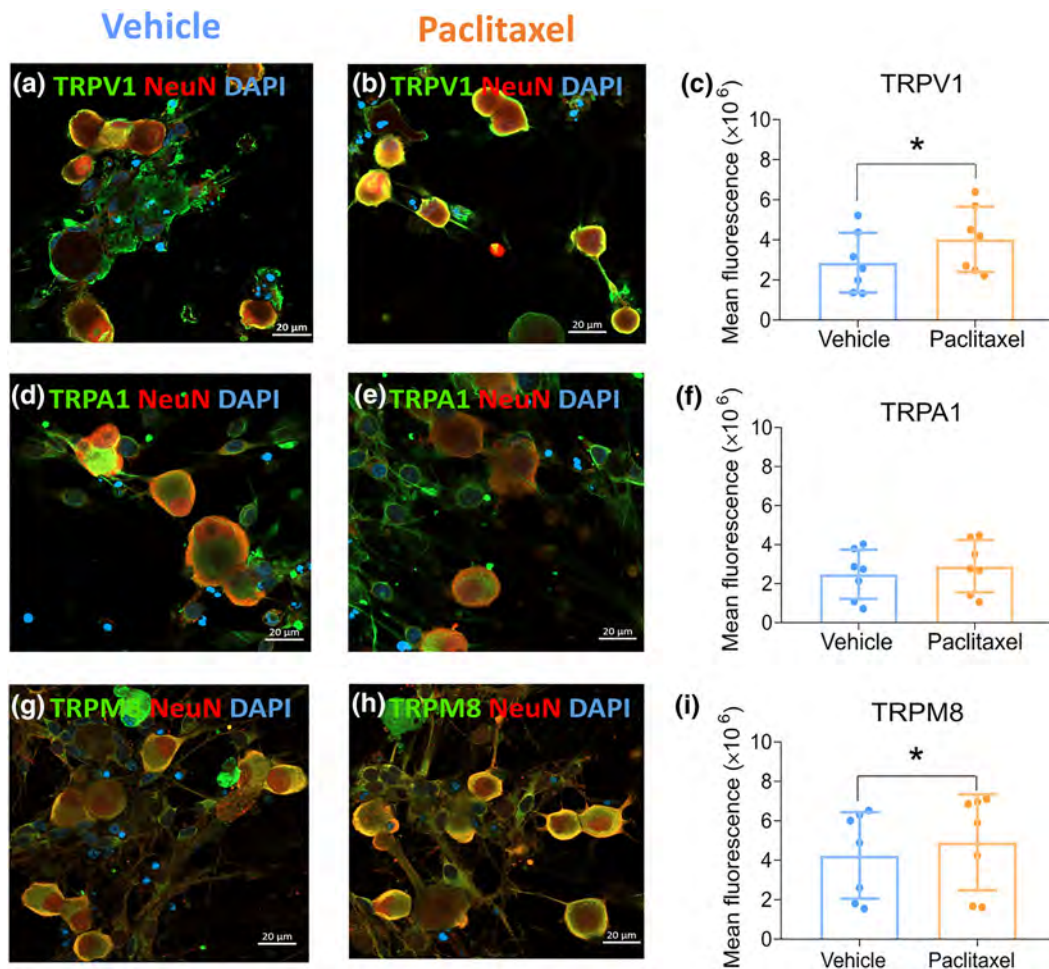


FIGURE 9 Paclitaxel increased immunoreactivity for TRPV1 and TRPM8 in sensory neurons. Immunocytochemical staining of cultured DRG neurons treated with vehicle or paclitaxel using anti-TRPV1, anti-TRPA1 or anti-TRPM8 antibodies along with the neuronal marker NeuN and DAPI staining. Green: TRPV1 (a, b), TRPA1 (d, e) or TRPM8 (g and h). Red: NeuN. DAPI: cyan. Scale bar denotes 20 μm. (c, f and i) Mean fluorescence intensity of TRPV1 (c), TRPA1 (f) or TRPM8 (i) immunoreactivity for vehicle and paclitaxel treated neurons. Data were collected 48 h post-treatment. Data are presented as individual values with means \pm SD; $N = 7$. * $P < 0.05$, significantly different from vehicle; paired t test

was potentiated. Analysis of the AP waveform indicated that electrogenic changes in IB4(−) were due to faster AP repolarization and to a faster and shallower AHP, while the effects observed in IB4(+) neurons resulted from down-regulation of the AHP amplitude. These results confirm that paclitaxel-induced electrogenic sensitization of DRG neurons does not require the participation of immune cells, although an autocrine action of IL-6 and CCK2 could be a contributory factor (Miller et al., 2009).

Several studies have shown an alteration of neural Na⁺ currents in CIPN due to paclitaxel (Nieto et al., 2008; Zhang & Dougherty, 2014) that mainly arises from an up-regulation of Nav1.7 channels in sensory neurons (Li et al., 2018). Na_v1.7 channels are TTX-sensitive channels displaying a hyperpolarized activation potential that contributes to set the AP threshold and the current rheobase in nociceptors (Dib-Hajj et al., 2005). Furthermore, the ratio of Na_v1.7: Na_v1.8 expression has been proposed to modulate the amplitude of subthreshold oscillations that may promote repetitive firing and control electrogenicity (Choi & Waxman, 2011). Na_v1.8 channels are TTX-resistant Nav channels

mainly involved in setting the upstroke of the AP, defining the inflection of the repolarization phase occurring in 60% of IB4(−) neurons, tuning the fast recovery from inactivation and contributing to the generation of resurgent Na⁺ currents (Renganathan et al., 2001; Xiao et al., 2019). Recent studies have shown that paclitaxel hyperexcitability could be blocked by the Na_v1.8-specific antagonist **A-803467** (Verma et al., 2020). Similarly, the work of Zhang et al. suggested that puerarin reduced paclitaxel induced neuropathic pain in rats by blocking the Na_v1.8 β1 subunit (Zhang et al., 2018). Our findings also point to Na_v1.8 channels in both nociceptor subtypes, as a central player of paclitaxel-induced neural excitability. The greater increase of Na_v1.8 channel activity in IB4(+) nociceptors treated with paclitaxel is consistent with the faster recovery of inactivation of Na⁺ ionic currents observed in these nociceptors. In support of this proposal, treatment of IB4(+) nociceptors with PF04885614 eliminated the faster recovery from inactivation provoked by paclitaxel. Intriguingly, in our model we did not observe any increase of Na_v1.7 channel activity, as reported in nociceptors from other animal models of

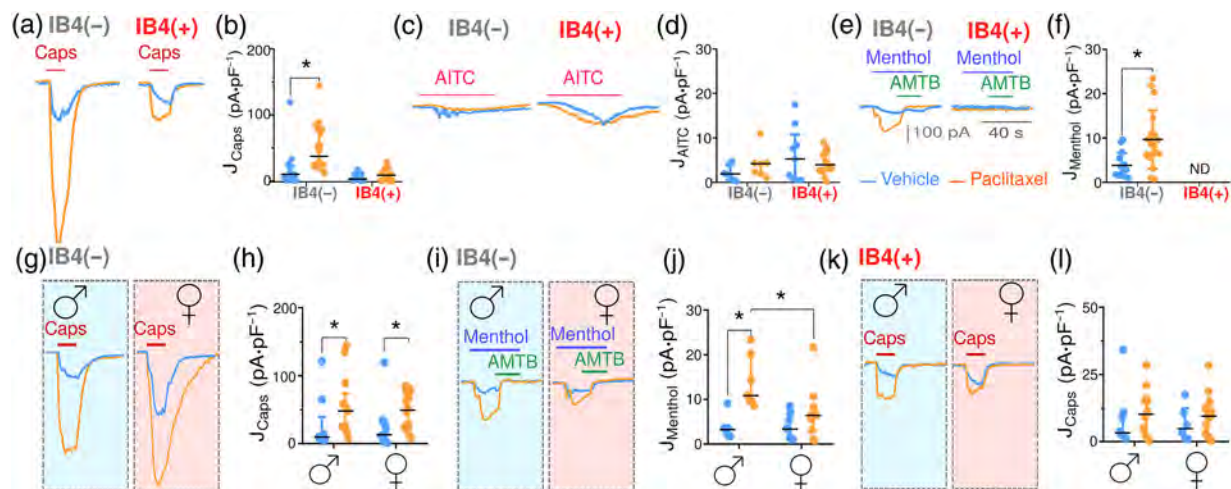


FIGURE 10 Paclitaxel increases TRPV1 and TRPM8 channel activity in IB4(-) neurons. (a, c and e) Representative inward current responses to a 1 μ M capsaicin (a), 100 μ M AITC (c) and 100 μ M menthol (e) of IB4(-) and IB4(+) neurons exposed to vehicle or paclitaxel. Calibration bars are for all recordings. TRPM8 channel activity was further confirmed by using the antagonist 10 μ M AMTB along with the menthol pulse. (b, d, and f) Peak current density observed after application of capsaicin (b), AITC (d) or menthol (f). AITC current was evoked in the same cells as capsaicin, after application of 4 capsaicin pulses. To quantify TRPM8 responses the remaining inward current during co-application of menthol and AMTB was subtracted from the peak response to menthol. Data are expressed as medians (with interquartile range) or as mean \pm SD. * P < 0.05, significantly different as indicated; Mann-Whitney test for capsaicin and AITC or unpaired t test for menthol. (g, i and k) Representative current responses to 1 μ M capsaicin (g) and 100 μ M menthol (i) for IB4(-) neurons and to capsaicin for IB4(+) (k) from male and female rats. (h) Quantitation of the current density in response to 1 μ M capsaicin revealed a similar potentiating effect of paclitaxel evoked in male DRG neurons, and their female counterparts. (j) Menthol-activated ionic currents were activated more potently in male IB4(-) DRG neurons ($N = 4$, $n = 7$), than in female IB4(-) neurons ($N = 4$, $n = 8$ for vehicle, $n = 11$ for paclitaxel). * P < 0.05, significantly different as indicated. (l) There was no significant effect of paclitaxel on the capsaicin-evoked currents in neurons from male rats ($N = 5$, $n = 8$ for vehicle and $n = 10$ for paclitaxel) or those from females ($N = 6$, $n = 6$ for vehicle and $n = 13$ for paclitaxel), although there was a trend towards an increase in both male and female cells. Recordings were made 48 h post-treatment. Data are presented as individual values with medians and interquartile ranges. * P < 0.05, significantly different as indicated; Kruskal-Wallis with Dunn's multiple comparisons test

paclitaxel-induced CIPN (Li et al., 2018; Xia et al., 2016). A possible explanation is that modulation of $\text{Na}_v1.7$ channel activity in nociceptors by paclitaxel may require the participation of proalgesic agents released from immune cells affected by the drug or/and that paclitaxel increased the axonal location of the channel (Akin et al., 2021). Thus, our findings suggest that $\text{Na}_v1.8$ channels are the major players defining the electrogenic properties following exposure to paclitaxel, including the threshold of action potential firing and the occurrence of repetitive firing (Choi et al., 2007; McDermott et al., 2019). Nonetheless, additional experiments are needed to define the contribution of $\text{Na}_v1.7$ and $\text{Na}_v1.9$ channels to setting the RMP and to regulate the neuronal excitability of different subpopulations of sensory neurons.

Electrogenicity is also defined by the AHP phase of the AP that is shaped by HCN (HCN1 and/or HCN2), K_{2P} and K_r channels. Down-regulation of K_{2P} and K_r channels would reduce the AHP amplitude depolarizing the RMP and increase neural excitability. Transcriptional analysis of DRGs from paclitaxel-treated mice showed a down-regulation of the mRNA for *KCN1* ($\text{K}_{v1.1}$) and *Kir3.4* (Zhang & Dougherty, 2014), which is consistent with the smaller AHP amplitude we observed. Because of their Na^+ permeability, HCN channels modulate AHP dynamics and electrogenic adaptation (Gu et al., 2005). An up-regulation of HCN channels reduces AHP amplitude and accelerates

restoration of RMP (Emery et al., 2012), thus promoting repetitive firing (Hogan & Poroli, 2008). Up-regulation of HCN2 channels has been shown in inflammatory and neuropathic pain conditions (Liu et al., 2018; Weng et al., 2012). Furthermore, a transcriptional increase of HCN1 mRNA expression was reported in an in vivo model of paclitaxel CIPN (Zhang & Dougherty, 2014), and HCN1 blockade attenuated oxaliplatin-induced CIPN (Resta et al., 2018). Accordingly, our finding that paclitaxel down-regulates AHP in IB4(-) and IB4(+) neurons suggests an up-regulation of HCN channels, most likely HCN1 (Zhang & Dougherty, 2014), although HCN2 cannot be fully ruled out. Collectively, our findings suggest that the effects of paclitaxel on IB4(-) and IB4(+) electrogenicity are due to regulation of Na_v and HCN channels, and probably K_{2P} and K_r channels. Nonetheless, we cannot discard regulation of other channels that also contribute to the AP waveform and electrogenicity, including Ca^{2+} -activated K^+ channels (BK, IK, SK) that are expressed in sensory neurons (Tsantoulas & McMahon, 2014). For instance, in IB4(-) neurons the faster AP repolarization may result from the up-regulation of a high-threshold K_A channel such as $\text{K}_{v4.3}$ that is a major contributor to K_A currents in IB4(-) nociceptors (Zemel et al., 2018). In IB4(+) neurons, AP repolarization could be influenced by the down-regulation of a low threshold K_A channel, such as $\text{K}_{v1.4}$ that is highly expressed in these neurons (Vydyanathan et al., 2005). Additional experiments are

needed to identify the ion channels altered by paclitaxel and to analyse how the drug affects their function (Malacrida et al., 2019).

We found that paclitaxel also up-regulated TRPV1 and TRPM8 channels, implying their contribution to heat and cold hypersensitivity in paclitaxel-evoked CIPN. Aligned with our findings, up-regulation of TRPV1 channel function by paclitaxel was previously observed and related to the burning pain that patients experience (Hara et al., 2013; Li et al., 2015). Our data suggest that paclitaxel-induced cold allodynia mainly arises from an up-regulation of TRPM8 channels. This result is consistent with a previous report showing that AMTB, a TRPM8 channel antagonist, reduced cold-hyperalgesia exhibited by paclitaxel-treated mice (Sałat & Filipek, 2015). However, our finding contrasts with the suggestion that paclitaxel-induced cold allodynia may be mediated by TRPA1 channels (Nazıroğlu & Braidy, 2017). A study in diabetic rats showed that paclitaxel up-regulated TRPA1 channels in sensory neurons and proposed a major role in cold allodynia in CIPN (Barrière et al., 2012). Intriguingly, we did not observe a direct effect of paclitaxel in the expression or function of TRPA1 channels. This discrepancy may arise from the different CIPN models used, as up-regulation of TRPA1 channels *in vivo* may be not due to the direct action of the drugs, but rather by algescic molecules released from immune cells (Materazzi et al., 2012; Viana, 2016).

Another relevant result of our preclinical *in vitro* nociceptor model is the finding that sensory neurons from females exhibit an apparently greater sensitivity to paclitaxel than those from males, suggesting a sex dimorphism. In contrast to the results in neurons from, paclitaxel provoked, in female neurons, a significant change in firing frequency, current rheobase and RMP depolarization, indicating a stronger drug-induced sensitization. However, sex-related differences in the electrogenic parameters did not reach statistical significance, most likely due to the modest sample size for the large phenotypic heterogeneity of nociceptors. Unexpectedly, we observed that paclitaxel promoted a higher up-regulation of TRPM8 channel activity in male sensory neurons than in females, while the effect on TRPV1 channel function was similar in both sexes. Studies in animal models have also reported the existence of sex dimorphism in paclitaxel CIPN, although these studies implied an immune-directed mechanism through TLR9-mediated nociceptor sensitization (Luo et al., 2019). Our findings additionally indicate that differences in sensitivity between male and female sensory neurons to paclitaxel are possible contributors to sex dimorphism. Studies that explore the sex prevalence of paclitaxel in humans also hint to higher prevalence in women, although the number of studies is limited, and these data need to be treated with caution (Kim et al., 2018). Nonetheless, the potential sex dimorphism in paclitaxel-induced sensitization of DRG neurons deserve further investigation and strongly supports the use of female animals in pre-clinical studies.

In conclusion, our preclinical, *in vitro*, model of paclitaxel-evoked CIPN provided insights of a direct drug effect on the electrogenic activity of IB4(−) and IB4(+) neurons. Our findings substantiate the use of pre-clinical *in vitro* models to investigate the direct effect of drugs on neural excitability, the underlying mechanisms and to unveil sex differences. *In vitro* models have the advantage of simplicity, compared with *in vivo* animal models that necessarily involve the

contribution of different cell types. However, as a trade-off, *in vitro* models for the highly heterogenous peripheral sensory system may favour cellular populations such as small sensory neurons or myelinated neurons depending on the trophic factors used for maturation (Höke et al., 2003). Nonetheless, models in a dish pave the way for using *in vitro* human sensory neurons reprogrammed from iPSC or transdifferentiated from fibroblasts (Blanchard et al., 2015; Chambers et al., 2012) as preclinical models to investigate the pathophysiology of peripheral neuropathies and to test drug candidates.

ACKNOWLEDGEMENTS

The authors thank C. Ferrándiz-Huertas for her technical assistance in immunocytochemistry experiments and J. De Andrés for her technical assistance with immunoblot experiments.

This study was funded by grants from AEI (MCIU) RTI2018-097189-B-C21 (to AFM and AFC) and from the Generalitat Valenciana (GVA) IDIFEDER2018/020 and PROMETEO/2021/031, co-funded with FEDER funds from EU “Una manera de hacer Europa,” and RTC-2017-6507-1 (to AFM), and a grant from the Universidad Miguel Hernández (UMH), PAR2019 (to AFM). EVR is a recipient of an UMH doctoral fellowship for research training (Ayuda para el apoyo a la formación del personal investigador).

AUTHOR CONTRIBUTIONS

EVR designed and performed the experiments, analysed the data, prepared the figures and revised the manuscript; RTM analysed the data, prepared and revised the figures and revised the manuscript; AFC revised the figures and manuscript; AFM revised the figures and data analysis, designed the experiments and wrote the manuscript.

CONFLICT OF INTEREST

Authors declare no conflict of interest.

DECLARATION OF TRANSPARENCY AND SCIENTIFIC RIGOUR

This Declaration acknowledges that this paper adheres to the principles for transparent reporting and scientific rigour of preclinical research as stated in the BJP guidelines for [Design and Analysis](#), [Immunoblotting and Immunochemistry](#), and [Animal Experimentation](#), and as recommended by funding agencies, publishers and other organizations engaged with supporting research.

DATA AVAILABILITY STATEMENT

The data that support the findings of this study are available from the corresponding author upon reasonable request.

ORCID

Eva Villalba-Riquelme  <https://orcid.org/0000-0002-0301-0672>

Roberto de la Torre-Martínez  <https://orcid.org/0000-0001-9872-6050>

Asia Fernández-Carvajal  <https://orcid.org/0000-0003-2741-1427>

Antonio Ferrer-Montiel  <https://orcid.org/0000-0002-2973-6607>

REFERENCES

- Abu Samaan, T. M., Samec, M., Liskova, A., Kubatka, P., & Büsselberg, D. (2019). Paclitaxel's mechanistic and clinical effects on breast cancer. *Biomolecules*, *9*(12), 789. <https://doi.org/10.3390/biom9120789>
- Akin, E. J., Alsalous, M., Higerd, G. P., Liu, S., Zhao, P., Dib-Hajj, F. B., Waxman, S. G., & Dib-Hajj, S. D. (2021). Paclitaxel increases axonal localization and vesicular trafficking of Nav1.7. *Brain*, *144*(6), 1727–1737. <https://doi.org/10.1093/brain/awab113>
- Alexander, S. P., Mathie, A., Peters, J. A., Veale, E. L., Striessnig, J., Kelly, E., Armstrong, J. F., Faccenda, E., Harding, S. D., Pawson, A. J., Southan, C., Davies, J. A., Aldrich, R. W., Attali, B., Baggetta, A. M., Becirovic, E., Biel, M., Bill, R. M., Catterall, W. A., ... Zhu, M. (2021). The concise guide to pharmacology 2021/22: Ion channels. *British Journal of Pharmacology*, *178*(Suppl 1), S157–s245. <https://doi.org/10.1111/bph.15539>
- Alexander, S. P. H., Roberts, R. E., Broughton, B. R. S., Sobey, C. G., George, C. H., Stanford, S. C., Cirino, G., Docherty, J. R., Giembycz, M. A., Hoyer, D., Insel, P. A., Izzo, A. A., Ji, Y., MacEwan, D. J., Mangum, J., Wonnacott, S., & Ahluwalia, A. (2018). Goals and practicalities of immunoblotting and immunohistochemistry: A guide for submission to the *British Journal of Pharmacology*. *British Journal of Pharmacology*, *175*(3), 407–411. <https://doi.org/10.1111/bph.14112>
- Barrière, D. A., Rieusset, J., Chanteranne, D., Busserolles, J., Chauvin, M. A., Chapuis, L., Salles, J., Dubray, C., & Morio, B. (2012). Paclitaxel therapy potentiates cold hyperalgesia in streptozotocin-induced diabetic rats through enhanced mitochondrial reactive oxygen species production and TRPA1 sensitization. *Pain*, *153*(3), 553–561. <https://doi.org/10.1016/j.pain.2011.11.019>
- Blanchard, J. W., Eade, K. T., Szűcs, A., Lo Sardo, V., Tsunemoto, R. K., Williams, D., Sanna, P. P., & Baldwin, K. K. (2015). Selective conversion of fibroblasts into peripheral sensory neurons. *Nature Neuroscience*, *18*(1), 25–35. <https://doi.org/10.1038/nn.3887>
- Chambers, S. M., Qi, Y., Mica, Y., Lee, G., Zhang, X. J., Niu, L., Bilsland, J., Cao, L., Stevens, E., Whiting, P., Shi, S. H., & Studer, L. (2012). Combined small-molecule inhibition accelerates developmental timing and converts human pluripotent stem cells into nociceptors. *Nature Biotechnology*, *30*(7), 715–720. <https://doi.org/10.1038/nbt.2249>
- Choi, J. S., Dib-Hajj, S. D., & Waxman, S. G. (2007). Differential slow inactivation and use-dependent inhibition of Nav1.8 channels contribute to distinct firing properties in IB4+ and IB4- DRG neurons. *Journal of Neurophysiology*, *97*(2), 1258–1265. <https://doi.org/10.1152/jn.01033.2006>
- Choi, J. S., & Waxman, S. G. (2011). Physiological interactions between Nav1.7 and Nav1.8 sodium channels: A computer simulation study. *Journal of Neurophysiology*, *106*(6), 3173–3184. <https://doi.org/10.1152/jn.00100.2011>
- Colvin, L. A. (2019). Chemotherapy-induced peripheral neuropathy: Where are we now? *Pain*, *160*(Suppl 1), S1–s10. <https://doi.org/10.1097/j.pain.0000000000001540>
- Curtis, M. J., Alexander, S., Cirino, G., Docherty, J. R., George, C. H., Giembycz, M. A., Hoyer, D., Insel, P. A., Izzo, A. A., Ji, Y., MacEwan, D. J., Sobey, C. G., Stanford, S. C., Teixeira, M. M., Wonnacott, S., & Ahluwalia, A. (2018). Experimental design and analysis and their reporting II: Updated and simplified guidance for authors and peer reviewers. *British Journal of Pharmacology*, *175*(7), 987–993. <https://doi.org/10.1111/bph.14153>
- da Costa, R., Passos, G. F., Quintão, N. L. M., Fernandes, E. S., Maia, J., Campos, M. M., & Calixto, J. B. (2020). Taxane-induced neurotoxicity: Pathophysiology and therapeutic perspectives. *British Journal of Pharmacology*, *177*(14), 3127–3146. <https://doi.org/10.1111/bph.15086>
- Dib-Hajj, S. D., Rush, A. M., Cummins, T. R., Hisama, F. M., Novella, S., Tyrrell, L., Marshall, L., & Waxman, S. G. (2005). Gain-of-function mutation in Nav1.7 in familial erythromelalgia induces bursting of sensory neurons. *Brain*, *128*(Pt 8), 1847–1854. <https://doi.org/10.1093/brain/awh514>
- Doyle, T., Chen, Z., Muscoli, C., Bryant, L., Esposito, E., Cuzzocrea, S., Dagostino, C., Ryerse, J., Rausaria, S., Kamadulski, A., Neumann, W. L., & Salvemini, D. (2012). Targeting the overproduction of peroxynitrite for the prevention and reversal of paclitaxel-induced neuropathic pain. *The Journal of Neuroscience*, *32*(18), 6149–6160. <https://doi.org/10.1523/jneurosci.6343-11.2012>
- Eldridge, S., Guo, L., & Hamre, J. 3rd. (2020). A comparative review of chemotherapy-induced peripheral neuropathy in in vivo and in vitro models. *Toxicologic Pathology*, *48*(1), 190–201. <https://doi.org/10.1177/0192623319861937>
- Emery, E. C., Young, G. T., & McNaughton, P. A. (2012). HCN2 ion channels: An emerging role as the pacemakers of pain. *Trends in Pharmacological Sciences*, *33*(8), 456–463. <https://doi.org/10.1016/j.tips.2012.04.004>
- Gu, N., Vervaeke, K., Hu, H., & Storm, J. F. (2005). Kv7/KCNQ/M and HCN/h, but not KCa2/SK channels, contribute to the somatic medium after-hyperpolarization and excitability control in CA1 hippocampal pyramidal cells. *The Journal of Physiology*, *566*(Pt 3), 689–715. <https://doi.org/10.1113/jphysiol.2005.086835>
- Hara, T., Chiba, T., Abe, K., Makabe, A., Ikeno, S., Kawakami, K., Utsunomiya, I., Hama, T., & Taguchi, K. (2013). Effect of paclitaxel on transient receptor potential vanilloid 1 in rat dorsal root ganglion. *Pain*, *154*(6), 882–889. <https://doi.org/10.1016/j.pain.2013.02.023>
- Hogan, Q. H., & Poroli, M. (2008). Hyperpolarization-activated current (I_h) contributes to excitability of primary sensory neurons in rats. *Brain Research*, *1207*, 102–110. <https://doi.org/10.1016/j.brainres.2008.02.066>
- Höke, A., Ho, T., Crawford, T. O., LeBel, C., Hilt, D., & Griffin, J. W. (2003). Glial cell line-derived neurotrophic factor alters axon schwann cell units and promotes myelination in unmyelinated nerve fibers. *The Journal of Neuroscience*, *23*(2), 561–567. <https://doi.org/10.1523/jneurosci.23-02-00561.2003>
- Kim, H. I., Lim, H., & Moon, A. (2018). Sex differences in cancer: Epidemiology, genetics and therapy. *Biomolecules & Therapeutics (Seoul)*, *26*(4), 335–342. <https://doi.org/10.4062/biomolther.2018.103>
- Li, Y., Adamek, P., Zhang, H., Tatsui, C. E., Rhines, L. D., Mrozkova, P., Li, Q., Kosturakis, A. K., Cassidy, R. M., Harrison, D. S., Cata, J. P., Sapire, K., Kenamer-Chapman, R. M., Jawad, A. B., Ghetti, A., Yan, J., Palecek, J., & Dougherty, P. M. (2015). The cancer chemotherapeutic paclitaxel increases human and rodent sensory neuron responses to TRPV1 by activation of TLR4. *The Journal of Neuroscience*, *35*(39), 13487–13500. <https://doi.org/10.1523/jneurosci.1956-15.2015>
- Li, Y., Marri, T., North, R. Y., Rhodes, H. R., Uhelski, M. L., Tatsui, C. E., Rhines, L. D., Rao, G., Corrales, G., Abercrombie, T. J., Johansson, C. A., & Dougherty, P. M. (2020). Chemotherapy-induced peripheral neuropathy in a dish: Dorsal root ganglion cells treated in vitro with paclitaxel show biochemical and physiological responses parallel to that seen in vivo. *Pain*, *162*, 84–96. <https://doi.org/10.1097/j.pain.0000000000002005>
- Li, Y., North, R. Y., Rhines, L. D., Tatsui, C. E., Rao, G., Edwards, D. D., Cassidy, R. M., Harrison, D. S., Johansson, C. A., Zhang, H., & Dougherty, P. M. (2018). DRG voltage-gated sodium channel 1.7 is upregulated in paclitaxel-induced neuropathy in rats and in humans with neuropathic pain. *The Journal of Neuroscience*, *38*(5), 1124–1136. <https://doi.org/10.1523/jneurosci.0899-17.2017>
- Lilley, E., Stanford, S. C., Kendall, D. E., Alexander, S. P. H., Cirino, G., Docherty, J. R., George, C. H., Insel, P. A., Izzo, A. A., Ji, Y., Panettieri, R. A., Sobey, C. G., Stefanska, B., Stephens, G., Teixeira, M., & Ahluwalia, A. (2020). ARRIVE 2.0 and the British Journal of Pharmacology: Updated guidance for 2020. *British Journal of Pharmacology*, *177*(16), 3611–3616. <https://doi.org/10.1111/bph.15178>
- Liu, X., Zhang, L., Jin, L., Tan, Y., Li, W., & Tang, J. (2018). HCN2 contributes to oxaliplatin-induced neuropathic pain through activation of the CaMKII/CREB cascade in spinal neurons. *Molecular Pain*, *14*, 1744806918778490. <https://doi.org/10.1177/1744806918778490>

- Luo, X., Huh, Y., Bang, S., He, Q., Zhang, L., Matsuda, M., & Ji, R. R. (2019). Macrophage toll-like receptor 9 contributes to chemotherapy-induced neuropathic pain in male mice. *The Journal of Neuroscience*, 39(35), 6848–6864. <https://doi.org/10.1523/jneurosci.3257-18.2019>
- Malacrida, A., Merzagalli, C., Rodriguez-Menendez, V., & Nicolini, G. (2019). Chemotherapy-induced peripheral neuropathy and changes in cytoskeleton. *International Journal of Molecular Sciences*, 20(9), 2287. <https://doi.org/10.3390/ijms20092287>
- Malgrange, B., Delr e, P., Rigo, J. M., Baron, H., & Moonen, G. (1994). Image analysis of neuritic regeneration by adult rat dorsal root ganglion neurons in culture: Quantification of the neurotoxicity of anti-cancer agents and of its prevention by nerve growth factor or basic fibroblast growth factor but not brain-derived neurotrophic factor or neurotrophin-3. *Journal of Neuroscience Methods*, 53(1), 111–122. [https://doi.org/10.1016/0165-0270\(94\)90151-1](https://doi.org/10.1016/0165-0270(94)90151-1)
- Markman, M. (1991). Taxol: An important new drug in the management of epithelial ovarian cancer. *The Yale Journal of Biology and Medicine*, 64(6), 583–590.
- Materazzi, S., Fusı, C., Benemei, S., Pedretti, P., Patacchini, R., Nilius, B., Prenen, J., Creminon, C., Geppetti, P., & Nassini, R. (2012). TRPA1 and TRPV4 mediate paclitaxel-induced peripheral neuropathy in mice via a glutathione-sensitive mechanism. *Pflügers Archiv*, 463(4), 561–569. <https://doi.org/10.1007/s00424-011-1071-x>
- McDermott, L. A., Weir, G. A., Themistocleous, A. C., Segerdahl, A. R., Blesneac, I., Baskozos, G., Clark, A. J., Millar, V., Peck, L. J., Ebner, D., Tracey, I., Serra, J., & Bennett, D. L. (2019). Defining the functional role of Na(V)1.7 in human nociception. *Neuron*, 101(5), 905–919.e908. <https://doi.org/10.1016/j.neuron.2019.01.047>
- McFarlane, S., & Cooper, E. (1991). Kinetics and voltage dependence of A-type currents on neonatal rat sensory neurons. *Journal of Neurophysiology*, 66(4), 1380–1391. <https://doi.org/10.1152/jn.1991.66.4.1380>
- Miller, R. J., Jung, H., Bhangoo, S. K., & White, F. A. (2009). Cytokine and chemokine regulation of sensory neuron function. *Handbook of Experimental Pharmacology*, (194), 417–449. https://doi.org/10.1007/978-3-540-79090-7_12
- Nazirođlu, M., & Braidı, N. (2017). Thermo-sensitive TRP channels: Novel targets for treating chemotherapy-induced peripheral pain. *Frontiers in Physiology*, 8, 1040. <https://doi.org/10.3389/fphys.2017.01040>
- Newberry, K., Wang, S., Hoque, N., Kiss, L., Ahljianian, M. K., Herrington, J., & Graef, J. D. (2016). Development of a spontaneously active dorsal root ganglia assay using multiwell multielectrode arrays. *Journal of Neurophysiology*, 115(6), 3217–3228. <https://doi.org/10.1152/jn.01122.2015>
- Nieto, F. R., Entrena, J. M., Cendán, C. M., Pozo, E. D., Vela, J. M., & Baeyens, J. M. (2008). Tetrodotoxin inhibits the development and expression of neuropathic pain induced by paclitaxel in mice. *Pain*, 137(3), 520–531. <https://doi.org/10.1016/j.pain.2007.10.012>
- Ohtsu, T., Sasaki, Y., Tamura, T., Miyata, Y., Nakanomyo, H., Nishiwaki, Y., & Saijo, N. (1995). Clinical pharmacokinetics and pharmacodynamics of paclitaxel: A 3-hour infusion versus a 24-hour infusion. *Clinical Cancer Research*, 1(6), 599–606.
- Percie du Sert, N., Hurst, V., Ahluwalia, A., Alam, S., Avey, M. T., Baker, M., Browne, W. J., Clark, A., Cuthill, I. C., Dirnagl, U., Emerson, M., Garner, P., Holgate, S. T., Howells, D. W., Karp, N. A., Lazic, S. E., Lidster, K., MacCallum, C. J., Macleod, M., ... Würbel, H. (2020). The ARRIVE guidelines 2.0: Updated guidelines for reporting animal research. *PLoS Biology*, 18(7), e3000410. <https://doi.org/10.1371/journal.pbio.3000410>
- Renganathan, M., Cummins, T. R., & Waxman, S. G. (2001). Contribution of Na(v)1.8 sodium channels to action potential electrogenesis in DRG neurons. *Journal of Neurophysiology*, 86(2), 629–640. <https://doi.org/10.1152/jn.2001.86.2.629>
- Resta, F., Micheli, L., Laurino, A., Spinelli, V., Mello, T., Sartiani, L., Di Cesare Mannelli, L., Cerbai, E., Ghelardini, C., Romanelli, M. N., Mannaioni, G., & Masi, A. (2018). Selective HCN1 block as a strategy to control oxaliplatin-induced neuropathy. *Neuropharmacology*, 131, 403–413. <https://doi.org/10.1016/j.neuropharm.2018.01.014>
- Satat, K., & Filipek, B. (2015). Antinociceptive activity of transient receptor potential channel TRPV1, TRPA1, and TRPM8 antagonists in neurogenic and neuropathic pain models in mice. *Journal of Zhejiang University. Science. B*, 16(3), 167–178. <https://doi.org/10.1631/jzus. B1400189>
- Schindelin, J., Arganda-Carreras, I., Frise, E., Kaynig, V., Longair, M., Pietzsch, T., Preibisch, S., Rueden, C., Saalfeld, S., Schmid, B., Tinevez, J. Y., White, D. J., Hartenstein, V., Eliceiri, K., Tomancak, P., & Cardona, A. (2012). Fiji: An open-source platform for biological-image analysis. *Nature Methods*, 9(7), 676–682. <https://doi.org/10.1038/nmeth.2019>
- Scuteri, A., Nicolini, G., Miloso, M., Bossi, M., Cavaletti, G., Windebank, A. J., & Tredici, G. (2006). Paclitaxel toxicity in post-mitotic dorsal root ganglion (DRG) cells. *Anticancer Research*, 26(2a), 1065–1070.
- Seretny, M., Currie, G. L., Sena, E. S., Ramnarine, S., Grant, R., MacLeod, M. R., Colvin, L. A., & Fallon, M. (2014). Incidence, prevalence, and predictors of chemotherapy-induced peripheral neuropathy: A systematic review and meta-analysis. *Pain*, 155(12), 2461–2470. <https://doi.org/10.1016/j.pain.2014.09.020>
- Smith, J. A., Slusher, B. S., Wozniak, K. M., Farah, M. H., Smiyun, G., Wilson, L., Feinstein, S., & Jordan, M. A. (2016). Structural basis for induction of peripheral neuropathy by microtubule-targeting cancer drugs. *Cancer Research*, 76(17), 5115–5123. <https://doi.org/10.1158/0008-5472.can-15-3116>
- Smith, S. B., Crager, S. E., & Mogil, J. S. (2004). Paclitaxel-induced neuropathic hypersensitivity in mice: Responses in 10 inbred mouse strains. *Life Sciences*, 74(21), 2593–2604. <https://doi.org/10.1016/j.lfs.2004.01.002>
- Son, S., Shim, D. W., Hwang, I., Park, J. H., & Yu, J. W. (2019). Chemotherapeutic agent paclitaxel mediates priming of NLRP3 inflammasome activation. *Frontiers in Immunology*, 10, 1108. <https://doi.org/10.3389/fimmu.2019.01108>
- Soriano, S., Gil-Rivera, M., Marroqui, L., Alonso-Magdalena, P., Fuentes, E., Gustafsson, J. A., Nadal, A., & Martinez-Pinna, J. (2019). Bisphenol A regulates sodium ramp currents in mouse dorsal root ganglion neurons and increases nociception. *Scientific Reports*, 9(1), 10306. <https://doi.org/10.1038/s41598-019-46769-6>
- Stucky, C. L., & Lewin, G. R. (1999). Isolectin B(4)-positive and -negative nociceptors are functionally distinct. *The Journal of Neuroscience*, 19(15), 6497–6505. <https://doi.org/10.1523/jneurosci.19-15-06497.1999>
- Tanay, M. A. L., Armes, J., & Ream, E. (2017). The experience of chemotherapy-induced peripheral neuropathy in adult cancer patients: A qualitative thematic synthesis. *European Journal of Cancer Care (Engl)*, 26(5), e12443. <https://doi.org/10.1111/ecc.12443>
- Tsantoulas, C., & McMahon, S. B. (2014). Opening paths to novel analgesics: The role of potassium channels in chronic pain. *Trends in Neurosciences*, 37(3), 146–158. <https://doi.org/10.1016/j.tins.2013.12.002>
- Verma, P., Eaton, M., Kienle, A., Flockerzi, D., Yang, Y., & Ramkrishna, D. (2020). Examining sodium and potassium channel conductances involved in hyperexcitability of chemotherapy-induced peripheral neuropathy: A mathematical and cell culture-based study. *Frontiers in Computational Neuroscience*, 14, 564980. <https://doi.org/10.3389/fncom.2020.564980>
- Viana, F. (2016). TRPA1 channels: Molecular sentinels of cellular stress and tissue damage. *The Journal of Physiology*, 594(15), 4151–4169. <https://doi.org/10.1113/jp270935>
- Vydyanathan, A., Wu, Z. Z., Chen, S. R., & Pan, H. L. (2005). A-type voltage-gated K⁺ currents influence firing properties of isolectin B4-positive but not isolectin B4-negative primary sensory neurons. *Journal of Neurophysiology*, 93(6), 3401–3409. <https://doi.org/10.1152/jn.01267.2004>

- Waxman, S. G., & Zamponi, G. W. (2014). Regulating excitability of peripheral afferents: Emerging ion channel targets. *Nature Neuroscience*, 17(2), 153–163. <https://doi.org/10.1038/nn.3602>
- Weng, X., Smith, T., Sathish, J., & Djouhri, L. (2012). Chronic inflammatory pain is associated with increased excitability and hyperpolarization-activated current (I_h) in C- but not A δ -nociceptors. *Pain*, 153(4), 900–914. <https://doi.org/10.1016/j.pain.2012.01.019>
- Xia, Z., Xiao, Y., Wu, Y., & Zhao, B. (2016). Sodium channel Nav1.7 expression is upregulated in the dorsal root ganglia in a rat model of paclitaxel-induced peripheral neuropathy. *Springerplus*, 5(1), 1738. <https://doi.org/10.1186/s40064-016-3351-6>
- Xiao, H., Verdier-Pinard, P., Fernandez-Fuentes, N., Burd, B., Angeletti, R., Fiser, A., Horwitz, S. B., & Orr, G. A. (2006). Insights into the mechanism of microtubule stabilization by Taxol. *Proceedings of the National Academy of Sciences of the United States of America*, 103(27), 10166–10173. <https://doi.org/10.1073/pnas.0603704103>
- Xiao, Y., Barbosa, C., Pei, Z., Xie, W., Strong, J. A., Zhang, J. M., & Cummins, T. R. (2019). Increased resurgent sodium currents in Nav1.8 contribute to nociceptive sensory neuron hyperexcitability associated with peripheral neuropathies. *The Journal of Neuroscience*, 39(8), 1539–1550. <https://doi.org/10.1523/jneurosci.0468-18.2018>
- Zajęczkowska, R., Kocot-Kępska, M., Leppert, W., Wrzosek, A., Mika, J., & Wordliczek, J. (2019). Mechanisms of chemotherapy-induced peripheral neuropathy. *International Journal of Molecular Sciences*, 20(6), 1451. <https://doi.org/10.3390/ijms20061451>
- Zemel, B. M., Ritter, D. M., Covarrubias, M., & Muqeem, T. (2018). A-type K(V) channels in dorsal root ganglion neurons: Diversity, function, and dysfunction. *Frontiers in Molecular Neuroscience*, 11, 253. <https://doi.org/10.3389/fnmol.2018.00253>
- Zhang, H., & Dougherty, P. M. (2014). Enhanced excitability of primary sensory neurons and altered gene expression of neuronal ion channels in dorsal root ganglion in paclitaxel-induced peripheral neuropathy. *Anesthesiology*, 120(6), 1463–1475. <https://doi.org/10.1097/aln.000000000000176>
- Zhang, X. L., Cao, X. Y., Lai, R. C., Xie, M. X., & Zeng, W. A. (2018). Puerarin relieves paclitaxel-induced neuropathic pain: The role of Na(v)1.8 β 1 subunit of sensory neurons. *Frontiers in Pharmacology*, 9, 1510. <https://doi.org/10.3389/fphar.2018.01510>

SUPPORTING INFORMATION

Additional supporting information may be found in the online version of the article at the publisher's website.

How to cite this article: Villalba-Riquelme, E., de la Torre-Martínez, R., Fernández-Carvajal, A., & Ferrer-Montiel, A. (2022). Paclitaxel in vitro reversibly sensitizes the excitability of IB4(–) and IB4(+) sensory neurons from male and female rats. *British Journal of Pharmacology*, 1–18. <https://doi.org/10.1111/bph.15809>